Parallel signaling through IRE1α and PERK regulates pancreatic neuroendocrine tumor growth and survival

Paul C. Moore[1,2,3,9], Jenny Y. Qi[1,2,3,9], Maike Thamsen[1,4,5,6], Rajarshi Ghosh[1,4,5,6], Micah J. Gliedt[4,5], Rosa Meza-Acevedo[1,4,5,6], Rachel E. Warren[1,2,3], Annie Hiniker[1,2,3], Grace E. Kim[1,2], Dustin J. Maly[7], Bradley J. Backes[4,5], Feroz R. Papa[1,3,4,5,6], Scott A. Oakes[1,2,3,8]

[1]Department of Pathology, [2]Helen Diller Family Comprehensive Cancer Center, [3]Diabetes Center, [4]Department of Medicine, [5]Lung Biology Center, [6]California Institute for Quantitative Biosciences, University of California, San Francisco, San Francisco, CA 94143, U.S.A. [7]Department of Chemistry, University of Washington, Seattle, WA 98195, U.S.A.

Correspondence:

feroz.papa@ucsf.edu (Tel: 415-476-2117)

scott.oakes@ucsf.edu (Tel: 415-476-1777)

[8] Lead Contact

[9] These authors contributed equally

Summary

Critical regulators of the unfolded protein response (UPR)—IRE1α and PERK— promote adaptation or apoptosis depending on levels of endoplasmic reticulum (ER) stress. While the UPR is activated in many cancers, its effects on tumor growth remain controversial. We used genetic and pharmacologic approaches to modulate IRE1α and PERK in cultured cells and xenograft and spontaneous genetic (RIP-Tag2) mouse models of pancreatic neuroendocrine tumors (PanNETs), highly secretory neoplasms prone to ER stress. We found that UPR signaling is optimized for adaptation and that inhibiting either IRE1α or PERK leads to hyperactivation and apoptotic signaling through the reciprocal arm, halting tumor growth and survival. Our results provide a strong rationale for therapeutically targeting the UPR in PanNETs and other cancers experiencing elevated ER stress.

Keywords

pancreatic neuroendocrine tumors, endoplasmic reticulum stress, unfolded protein response, IRE1α, PERK, *K*inase *I*nhibiting *R*Nase *A*ttenuators, PERK kinase inhibitor, apoptosis

Significance

For the nearly 1,500 Americans diagnosed with PanNETs annually, surgery is the only potentially curative treatment. Unfortunately, the five-year survival is extremely low for the ~25% of patients who develop metastatic disease. Derived from pancreatic endocrine cells, PanNETs universally hypersecrete one or more peptide hormones, likely sensitizing them to ER protein-folding stress. Accordingly, we analyzed human PanNET samples and found evidence of elevated ER stress and UPR activation. Importantly, genetic and pharmacological inhibition of the IRE1α or PERK pathways in two preclinical PanNET models led to compensatory hyperactivation of the reciprocal arm and impaired tumor survival and growth. Our results provide new mechanical insight and strong rationale for targeting the UPR in neoplasms with elevated ER stress.

Introduction

Over a third of all proteins in the mammalian cell, including nearly all secreted proteins, are co- or post-translationally translocated into the endoplasmic reticulum (ER) where they are then folded and modified by chaperones, glycosylating enzymes, oxido-reductases, and other ER-localized enzymes (Sevier and Kaiser, 2002; Tu and Weissman, 2004). Incompletely folded proteins are eliminated by quality control systems, including ER-associated degradation (ERAD) pathways (McCracken and Brodsky, 2003; Meusser et al., 2005; Smith et al., 2011). When misfolded proteins in the ER accumulate above a critical threshold, a corrective intracellular signaling pathway called the unfolded protein response (UPR) is initiated to restore homeostasis. The UPR is controlled by three ER transmembrane proteins—inositol-requiring enzyme 1α (IRE1α; also known as ERN1), PKR-like ER kinase (PERK; also known as EIF2AK3), and activating transcription factor 6 (ATF6)—that detect misfolded proteins and induce transcriptional and translational upregulation of components to expand ER protein folding capacity and decrease protein folding demand (Hetz et al., 2015; Lerner et al., 2012; Meusser et al., 2005; Shore et al., 2011; Smith et al., 2011). If ER stress levels are too severe or prolonged to restore homeostasis, the UPR regulators switch from pro-homeostatic to pro-apoptotic outputs (Oakes and Papa, 2015).

The most ancient UPR sensor, IRE1α, contains an ER lumenal domain that recognizes unfolded proteins and consequently undergoes dimerization or oligomerization depending on the degree of lumenal engagement (Aragon et al., 2009; Credle et al., 2005; Zhou et al., 2006). The cytosolic face of IRE1α has two distinct enzymatic domains—a serine/threonine kinase and an endoribonuclease (RNase). Remediable ER stress

causes dimerization and subsequent *trans*-autophosphorylation of the kinase domain, which allosterically activates the attached RNase to initiate frame-shift splicing of *XBP1* mRNA. Excision of a 26nt intron allows translation of the XBP1s (s=spliced) transcriptional factor, which upregulates genes encoding ER protein-folding and quality control components (Kosmaczewski et al., 2014; Lu et al., 2014). Analogously, recognition of misfolded proteins by the lumenal domain of PERK results in dimerization, *trans*-autophosphorylation and activation of its cytosolic kinase domain (Cui et al., 2011; Harding et al., 1999). In turn, PERK phosphorylates eIF2α, leading to downregulation of Cap-dependent translation in order to reduce protein load on the ER (Ron and Walter, 2007; Shi et al., 1998). Concurrently, transcripts with upstream open reading frames (uORFs), such as Activating Transcription Factor 4 (ATF4), are preferentially translated and further promote ER protein folding and quality control (Young and Wek, 2016). Collectively, remediable UPR signaling culminates in the "*Adaptive (A)-UPR,*" which, if successful, restores ER homeostasis (Lee et al., 2003).

Under sustained, irremediable ER stress, high-level kinase autophosphorylation causes IRE1α oligomerization and relaxed specificity of its RNase, allowing it to endonucleolytically degrade many ER membrane-localized mRNAs that encode secretory proteins, such as pro-insulin, as well as essential components of the ER-resident protein-folding machinery (Han et al., 2009; Hollien et al., 2009). This activity, which has been termed *R*egulated *I*RE1-*D*ependent *D*ecay of mRNA (RIDD), results in deterioration of ER function (Han et al., 2009). Moreover, hyperactivated IRE1α degrades select microRNA precursors to upregulate key apoptotic signals, including Thioredoxin-Interacting Protein (TXNIP) (Lerner et al., 2012; Upton et al., 2012). Similarly, prolonged

PERK activation results in upregulation of the transcription factor CHOP/GADD153, which attenuates expression of anti-apoptotic BCL-2 and increases expression of pro-apoptotic BCL2 family proteins to promote cell death (Marciniak et al., 2004; McCullough et al., 2001). The net result is induction of a "*Terminal (T)-UPR*," whereby adaptive signaling through XBP1s and ATF4 is eclipsed by pro-apoptotic signals (Fig 1A).

Cancer cells often invade foreign environments where unfavorable conditions such as hypoxia and nutrient deprivation compromise protein folding in the ER (Koumenis, 2006; Lee and Hendershot, 2006; Ma and Hendershot, 2004; Moenner et al., 2007; Oakes, 2017). As such, elevated ER stress and UPR activity have been documented in various solid cancers, such glioblastoma and carcinomas of the breast, stomach, esophagus, and liver (Carrasco et al., 2007; Chen et al., 2002; Fernandez et al., 2000; Gardner and Walter, 2011; Shuda et al., 2003; Song et al., 2001). However, whether the UPR ultimately inhibits or promotes tumor growth remains an area of intense debate (Auf et al., 2010; Bobrovnikova-Marjon et al., 2010; Jamora et al., 1996; Oakes, 2017; Park et al., 2004; Romero-Ramirez et al., 2004).

We speculated that pancreatic neuroendocrine tumors (PanNETs), which are characterized by a high secretory load, might be particularly sensitive to protein-folding stress. Derived from endocrine cells, PanNETs universally *hyper*-secrete one or more polypeptide hormones such as insulin or glucagon (Metz and Jensen, 2008; Oberg and Eriksson, 2005). Moreover, the development and maintenance of pancreatic neuroendocrine cells is greatly impacted by genetic loss of the UPR in mice and humans (Delepine et al., 2000; Hassler et al., 2015; Lee et al., 2011).

Here we show that ER stress-induced activation of the Adaptive-UPR is strongly upregulated in human PanNET samples and in two distinct murine models. Using genetic tools, we discovered that disruption of the Adaptive-UPR or activation of the Terminal-UPR is detrimental to PanNET growth and survival *in vivo*. Likewise, administration of highly selective IRE1α and PERK kinase inhibitors in two murine preclinical PanNET models phenocopies the antitumor effects of genetic deletion. Specifically, we find that inhibiting IRE1α or PERK exacerbates ER stress and leads to compensatory apoptotic signaling through the reciprocal UPR branch. In particular, pharmacological targeting of IRE1α increased life expectancy without deleterious effects on animal health, highlighting its promise as a therapeutic target in PanNETs and other ER stress-sensitive cancers.

Results

Primary Human PanNETs and a Xenograft PanNET Model Show Evidence of Elevated ER Stress

To look for markers of ER stress and UPR activation, we obtained a panel of six human PanNETs from the UCSF Department of Pathology and performed immunohistochemistry (IHC) against the ER chaperone BiP/GRP78, which is upregulated by the adaptive UPR when misfolded proteins accumulate in the ER. We observed markedly higher expression in 5 of the 6 human PanNETs compared with normal pancreas (Fig 1B-C, S1A), indicating an elevated level of ER protein-folding stress in these tumors. Moreover, we found that *XBP1* splicing (a readout for IRE1α signaling) and *ATF4* mRNA expression (a readout for PERK signaling) were both upregulated in human PanNETs compared with normal pancreas (Fig 1D-E).

To recapitulate UPR signaling *in vivo*, we employed an established PanNET xenograft mouse model using rat insulinoma (INS-1) cells, which are one of the most widely employed PanNET lines because they secrete insulin in response to glucose (Asfari et al., 1992; Babu et al., 2013). To do so, we injected 5 million INS-1 cells subcutaneously (s.c.) into the flank of immunodeficient NOD-*scid* IL2Rgamma^{null} (NSG) mice (Fig 1F). Tumors became palpable at 1-2 weeks post-injection and closely resembled human PanNETs by histology and IHC, staining for known markers, including insulin, chromogranin A (CgA), and synaptophysin (SPH) (Fig 1G-J). Moreover, CD31 staining demonstrated that the INS-1 xenografts showed similar vascular patterns compared with human PanNETs (Fig 1K). Notably, in comparison to the same INS-1 cells

grown *in vitro*, INS-1 xenograft tumors displayed marked upregulation of IRE1α (XBP1s) and PERK (p-PERK) signaling (Fig 1L). Together, these data demonstrate that *in vivo* PanNETs have an elevated level of adaptive UPR signaling, which we hypothesized may allow them to accommodate high protein-folding demand and avoid ER stress-induced toxicity.

Manipulation of IRE1α Adaptive vs. Apoptotic Signaling Determines Growth of INS-1 Xenograft Tumors

Previously, we engineered transgenic INS-1 cell lines that express Tet repressor and are stably integrated with Doxycycline (Dox)-inducible constructs of Myc-tagged IRE1α (Han et al., 2009; Shuda et al., 2003). *In vitro*, addition of Dox leads to supraphysiological production of transgenic IRE1α, which oligomerizes through mass action and *trans*-autophosphorylates, activating the RNase to induce *Xbp1* splicing, ER-localized mRNA decay, and a Terminal UPR (Han et al., 2009). To test the effects of IRE1α hyperactivation on tumor growth and survival *in vivo*, we adapted this system to manipulate expression of murine IRE1α in the INS-1 xenograft model.

We injected equal numbers of Dox-inducible INS-1 (vector) and INS-1::IRE1α cells into the flanks of NSG mice and provided either regular or Dox chow to control transgene expression (Fig 1F). Dox chow alone had no effect on the size of control INS-1 tumors over a 4-week time course; in contrast, Dox-induced overexpression and hyperactivation of IRE1α markedly reduced tumor mass to <30% of INS-1 control tumors (Fig 2A-C, S2A). This reduction in INS-1 tumor burden upon IRE1α hyperactivation was associated with significant increases in both adaptive (*Xbp1s*; Fig 2D, S2B) and apoptotic outputs

(elevation of *Txnip*, and decrements in *Ins1* and *Ins2*; Fig 2E-G, S2C-D). Furthermore, short-term expression of IRE1α was sufficient to induce robust apoptosis as visualized by cleaved Caspase-3 staining (Fig 2H-I). These findings are consistent with our *in vitro* observations that the Terminal UPR eventually eclipses XBP1s-dependent adaptive signaling to trigger apoptosis (Ghosh et al., 2014; Han et al., 2009).

Intriguingly, INS-1::IRE1α tumors were consistently larger than the INS-1 vector controls in the absence of Dox (Fig 2A). The most likely explanation for this result is that leaky expression of the *Ire1α* transgene (Fig 2B-C, S2A) promoted a modest increase in *Xbp1* splicing without significantly altering IRE1α's apoptotic outputs, as we had found in *vitro* (Fig 2D-I, S2B-D; (Han et al., 2009)). This result further demonstrates that the balance of adaptive and apoptotic signals downstream of IRE1α is optimized by PanNETs to favor their growth and avert cell death. This suggested that IRE1α could be manipulated to impact tumor growth and survival.

CRISPR/Cas9-mediated Knockout of IRE1α or PERK Pathway Dramatically Decreases INS-1 Tumor Burden

Just as hyperactivation of IRE1α unbalances UPR signaling and impairs tumor development, we reasoned that inhibition of UPR pathways would have a similar effect on impeding tumorigenesis. To initially test this concept, we used the CRISPR/Cas9 gene editing system to functionally knock out *Ire1α*, *Xbp1*, and *Perk* in INS-1 cells. For each target, two distinct guide RNAs (gRNA) were used to induce random insertions/deletions (indels) upstream of key structural and functional domains. Clonal lines were isolated from each gRNA and knockout (KO) and confirmed by genotyping and Western blot (Fig 3A).

We injected equal numbers of INS-1 KO clones and parental INS-1 cells into NSG mice and allowed tumors to develop for 4 weeks. Strikingly, all UPR KO clones showed markedly impaired tumor growth, in some cases attaining only ~10% of the mass of control INS-1 tumors (Fig 3C-H). This correlated with a >65% reduction of actively proliferating cells, as determined by Ki67 staining (Fig 3I-J). Conversely, INS-1 cells subjected to scrambled (Scr) CRISPR/Cas9 controls achieved a tumor mass no different from that of the parental INS-1 cells, confirming that the CRISPR/Cas9 clonal selection procedure does not grossly affect xenograft compatibility (Fig S3A).

Interestingly, proliferation and survival rates of cultured INS-1 KO lines were not diminished in comparison to the parental INS-1 cells (Fig 3B), suggesting that full UPR functionality is dispensable *in vitro*. As previously shown, INS-1 xenograft tumors have elevated IRE1α and PERK signaling (Fig 1L), indicative of a high-stress environment *in vivo*. In that context, this observed discrepancy between growth of UPR KO lines in culture and in an animal further underscores the role of the UPR in buffering environmental stress and promoting tumor growth *in vivo*.

Pharmacological Inhibitors of IRE1α and PERK Increase Sensitivity to ER Stress-Induced Apoptosis *In Vitro*

Although the aforementioned genetic models highlight the importance of the UPR in tumor growth, the development of potent and highly selective small-molecule inhibitors against these UPR stress sensors provides a unique opportunity to further dissect their roles in tumorigenesis and discern their potentials for pharmaceutical intervention.

Our team developed first-in-class ATP-competitive IRE1α *K*inase *I*nhibiting *R*Nase *A*ttenuators—*KIRAs*—that bind IRE1α's kinase domain and allosterically inhibit its RNase

(Feldman et al., 2016; Ghosh et al., 2014). Recently, a more potent and selective KIRA series was published that had no effect on cell viability when administered to a large panel of cultured non-PanNET tumor cell lines for 48h (Harrington et al., 2015). This result is consistent with our findings that IRE1α activity is relatively low in cultured cells (Fig 1L) and that both IRE1α KO and XBP1 KO cells grow equivalently to INS-1 cells *in vitro* (Fig 3B). We re-synthesized a monoselective IRE1α inhibitor from this series (compound 18), which has recently been renamed KIRA8 (Fig 4A) (Morita et al., 2017). Not only did KIRA8 fail to inhibit any of the other >365 kinases tested *in vitro*, it is so selective against IRE1α that it minimally inhibits the closely related paralog, IRE1β (Morita et al., 2017). Administration of KIRA8 to cultured INS-1 cells revealed an IC_{50} of ~125 nM; doses between 500 nM and 1 μM resulted in near-complete inhibition of *Xbp1* splicing, reversal of RIDD (*Ins1* mRNA decay), and prevention of apoptosis due to enhanced (Dox-induced) IRE1α signaling (Fig 4B; S4A-B).

Correspondingly, we obtained a highly selective PERK inhibitor—GSK2656157—that is referred to here as *GSK-P*ERK *K*inase *I*nhibitor (GSK-PKI; Fig 4C) (Atkins et al., 2013). Similarly to KIRA8, GSK-PKI displayed minimal off-target inhibition against a panel of 300 kinases *in vitro*, including other eIF2α kinases (Atkins et al., 2013). Under conditions of elevated ER stress in cultured INS-1 cells, GSK-PKI also exhibited an IC_{50} of ~125 nM with near-optimal inhibition of PERK autophosphorylation and expression of the pro-apoptotic factor CHOP between 500 nM and 1 μM (Fig 4D).

Even at doses that essentially eliminate *Xbp1* splicing, long-term exposure of cultured INS-1 cells to KIRA8 neither affected their viability (Fig 4E) nor their proliferation (Fig 4G). Conversely, GSK-PKI treatment mildly increased apoptosis and dampened

growth rate in cultured INS-1 cells (Fig 4F and G). Regardless, whether this discrepancy stems from pathway compensation in PERK KO cells or off-target effects from the GSK-PKI compound (Rojas-Rivera et al., 2017), the aggregate effect is modest in cells with low ER stress.

Just as tumor environment necessitates UPR signaling *in vivo*, we hypothesized that inducing ER stress in INS-1 cells *in vitro* would sensitize them to treatments with KIRA8 and GSK-PKI. Therefore, we mildly induced ER stress and activated both IRE1α and PERK pathways using thapsigargin (inhibitor of ER Ca^{2+} pump; Fig 5D, S5A) alone or in combination with 500 nM of KIRA8 or GSK-PKI. In the presence of ER stress, the addition of either inhibitor roughly doubled the number of apoptotic cells over 30 hours of treatment (Fig 5A).

Because inhibition of one UPR pathway impairs its adaptive stress response, this may worsen ER stress and cause compensatory hyperactivation of and apoptotic signaling from the remaining UPR pathway. To explore this possibility, we monitored IRE1α and PERK pathway activation in response to thapsigargin, in the presence or absence of KIRA8 or GSK-PKI. While treatment with KIRA8 did not have a noticeable effect on PERK autophosphorylation, high baseline levels may have masked any subtle changes (Fig 5B). However, KIRA8 further increased thapsigargin-induced CHOP expression, implying that PERK activity had indeed increased (Fig 5B). To further elucidate this mechanism, we tested the ability of INS-1 cells to recover from induced ER stress in the presence or absence of KIRA8. Indeed, KIRA8-mediated inhibition of IRE1α led to sustained p-PERK and CHOP levels after thapsigargin washout (Fig 5C).

Congruently, treatment with GSK-PKI boosted *Xbp1* splicing both with and without ER stress induction, indicating compensation through IRE1α (Fig 5D).

Pharmaceutical Inhibition of IRE1α or PERK Impedes Growth and Induces Apoptosis of INS-1 Tumors

We next tested the effectiveness of pharmacologic UPR inhibitors *in vivo* using the INS-1 xenograft model. To do so, we formulated vehicles specific to KIRA8 and GSK-PKI and administered intraperitoneal injections (i.p.) of each drug (50 mg/kg/day) estimated to achieve a serum concentration above its IC_{50}. Tumors were grown in NSG mice for two weeks, treated for 48 hours, harvested and analyzed for target inhibition by their respective drugs. Dosing with KIRA8 lowered *Xbp1* splicing from a baseline of ~15% to below 1.5% (Fig 6A; S6A); GSK-PKI treatment reduced PERK autophosphorylation below detectable levels (Fig 6B), confirming *in vivo* target engagement for both compounds.

To determine the effects on tumor burden, we injected NSG mice with INS-1 cells as previously described and administered daily doses of KIRA8 or GSK-PKI and the respective vehicle in parallel for three weeks prior to harvest. While the decreases in tumor size were less dramatic than CRISPR/Cas9-directed KO of IRE1α or PERK, both KIRA8 and GSK-PKI significantly reduced tumor mass by ~50% (Fig 6C-F). Once again, this stands in sharp contrast to the lack of efficacy of these compounds on INS-1 growth *in vitro* (Fig 4E-G), except when ER stress is induced chemically (Fig 5A).

To explore the mechanistic causes of decreased tumor burden, we next examined whether *in vivo* inhibition of IRE1α or PERK affects PanNET tumor growth and/or survival. In contrast to cultured INS-1 cells, INS-1 tumors exhibited markedly decreased Ki67

staining within 48 hours of KIRA8 or GSK-PKI administration *in vivo* (Fig 7A-D). More specifically, KIRA8 and GSK-PKI appear to block G_1-S transition by impairing expression of Cyclin E1 and D1, respectively (Fig S7A-B).

Moreover, *in vivo* administration of either compound increased levels of Cleaved Caspase-3 roughly 1.5-fold (Fig 7E-H). Due to high basal PERK activation *in vivo*, we were unable to directly detect further increases in PERK autophosphorylation under KIRA8 treatment (Fig S7C), but did note increased levels of PERK-associated markers for ER stress (*Bip*, *Ire1*α) and apoptosis (*Txnip*, *Bim*; Fig 7I) (Lerner et al., 2012; Luo et al., 2003; Puthalakath et al., 2007; Tsuru et al., 2016). Importantly, *Ire1*α and *Bim* are inversely regulated by GSK-PKI (Fig S7D).

In regard to GSK-PKI, cytotoxicity was associated with increased *Xbp1* splicing (Fig 7J, S7E) and decreases in *Ins1* and *Ins2* mRNA (Fig 7K), implicating upregulation of adaptive and pro-apoptotic (RIDD) IRE1α signaling, respectively. Our observation that *Ins1* and *Ins2* mRNA levels are unaffected in KIRA8-treated cells despite elevated ER stress and apoptosis further supports this association between PERK inhibition and RIDD (Fig S7F).

KIRA8 Treatment Decreases Tumor Size and Prolongs Survival in a RIP-Tag2 PanNET Model

In light of the critical role of the UPR for tumor growth in the INS-1 xenograft model, we decided to test the effects of KIRA8 and GSK-PKI in a second preclinical PanNET model. The RIP-Tag2 (RT2) mouse is a transgenic strain in which viral SV40 large T-antigen (Tag) expression is driven by the rat insulin promoter-1 (RIP) (Hanahan, 1985). This

mouse has been extensively used as a model of endogenous pancreatic neuroendocrine tumorigenesis due to β-cell specific expression of the Tag oncogene and predictable development of islet hyperplasia (5-10wks), adenomas (10-12 wks), and eventually invasive and/or metastatic disease (12-15 wks) (Bergers et al., 1999)(Fig 8A). Similar to the INS-1 xenograft model, RIP-Tag2 pancreata also display elevated ER stress in comparison to wild-type (WT) controls (Fig 8B-C).

To best replicate clinical conditions, we performed a tumor regression trial: we began vehicle or drug (50mg/kg daily i.p. of KIRA8 or GSK-PKI) administration at 12 weeks of age, which is when tumors have become invasive and/or metastatic (Fig 8A), and continued therapy for 14 days. After the 2-week treatment period, we sacrificed the animals and fixed their pancreata for H&E staining to measure tumor burden as a percentage of total pancreas area (Fig 8D-E). In KIRA8-treated animals, tumor burden was decreased >75% when compared with vehicle-treated control animals (Fig 8D and F); otherwise, there were no visibly detrimental effects on the surrounding pancreas. GSK-PKI also reduces tumor burden (~50%) in the RIP-Tag2 model but was associated with widespread degeneration of the exocrine pancreas (Fig 8E and G).

The deleterious impact of GSK-PKI on pancreatic health spurred us to closely compare the effects of both compounds on wild-type mice. Twelve-week old C57BL/6 mice were treated for 14 days with vehicle, KIRA8, or GSK-PKI at 50mg/kg before sacrificing and removing the pancreas. KIRA8 had no discernible effects on pancreas health or mass (Fig 8H; S8A), whereas GSK-PKI treatment resulted in severe disruption of the exocrine pancreas and a corresponding ~50% loss of pancreas mass (Fig 8I; S8B).

Based on these data, we focused on KIRA8 and performed a survival study following initiation of treatment at 12 weeks of age. Impressively, while the vehicle-treated animals lived an average of 17 days after initiation of treatment, the KIRA8 animals survived over twice as long, with several animals surviving over 60 days and 1 animal up to 82 days (Fig 8J). Aside from some mild irritation at the injection site, the KIRA8-treated animals showed no other adverse effects for the duration of the experiment.

Discussion

Currently, PanNETs are only potentially curable through surgical resection. For the 20-30% of patients who have distant metastases at diagnosis, treatment is limited to managing symptoms of hormonal hypersecretion and administering systemic chemotherapy, to which the tumor invariably develops resistance. The 5-year survival for these patients is as low as 4-25% (van der Zwan et al., 2013; Yao et al., 2008). Treatments with targeted therapies, such as the FDA-approved drugs everolimus (an mTOR inhibitor) and sunitinib (a multi-kinase inhibitor), only have relatively modest benefits (~6 month increase in progression-free survival) in patients with metastatic PanNETs (Raymond et al., 2011; Yao et al., 2011). Most recently, peptide receptor radiotherapy (PRRT) has shown highly promising outcomes in clinical trials for some patients with metastatic somatostatin receptor (SSTR)-expressing PanNETs, but the fraction of patients who respond and the long-term outcomes remain unknown (Cives and Strosberg, 2017). As such, there continues to be urgent need for greater insight into the molecular biology of PanNETs and the development of better therapies.

Notably, the professional secretory cells of the endocrine pancreas that PanNETs originate from are critically dependent on the UPR for their development and survival. Homozygous deletion of the *Perk* gene in mice causes IRE1α hyperactivation, massive β-cell apoptosis, diabetes, pancreatic exocrine insufficiency, and early growth defects (Delepine et al., 2000; Harding et al., 2000). This phenocopies Wolcott-Rallison syndrome, a rare human infantile diabetic syndrome caused by homozygous loss-of-function *PERK* mutations. Similarly, the genetic removal of *Ire1*α in adult β-cells results in their severe dysfunction and defective insulin secretion (Hassler et al., 2015), whereas deleting *Xbp1*

in the β-cell compartment leads to upstream IRE1α hyperactivation, degeneration of β-cells, and hyperglycemia (Lee et al., 2011). However, it is likely that PanNETs are even more dependent on the UPR as they constitutively hypersecrete one or more hormones (Metz and Jensen, 2008; Oberg and Eriksson, 2005). For instance, some “insulinoma” PanNET cells secrete over 10-fold higher amounts of insulin than normal pancreatic β-cells, even under hypoglycemic conditions (Scheuner and Kaufman, 2008). Even clinically silent “nonfunctioning” PanNETs usually secrete high levels of multiple hormones and peptides that do not cause clinical symptoms (Baudin et al., 1998; Nobels et al., 1998; Pirker et al., 1998). Based on these observations, we predicted that PanNETs would be particularly dependent on the UPR to manage ER stress under the weight of their high secretory protein load.

As anticipated, we observed elevated markers for ER stress and UPR activation in both human PanNETs and two murine models of the disease. Importantly, we found INS-1 cells grown in culture have low levels of ER stress and UPR activation; however, the same cells grown in mice as xenografts show marked activation of the UPR. These results demonstrate the unique challenges to ER proteostasis (e.g., hypoxia, nutrient deprivation) that cancer cells encounter *in vivo* that are not mimicked by cell culture conditions. In keeping with the minimal UPR activation seen in cultured INS-1 cells, neither genetic deletion nor pharmacological blockade of IRE1α or PERK pathways had any profound effects on INS-1 growth *in vitro*. These results are consistent with the lack of cytotoxicity observed when the IRE1α inhibitor KIRA8 was applied to a range of cultured cancer cell lines (Harrington et al., 2015).

The INS-1 PanNET xenografts containing a doxycycline-inducible IRE1α provided the first evidence that the level of IRE1α activation has important consequences for tumor growth *in vivo*. Frank overexpression and hyperactivation of IRE1α induced RIDD and resulted in massive apoptosis; in contrast, "leaky," low-level IRE1α overexpression enhanced adaptive signaling through XBP1s and promoted tumor growth.

To further test the dependency of PanNETs on UPR signaling, we used loss of function approaches. Consistent with this notion, IRE1α or PERK inhibition in INS-1 xenograft PanNET models markedly impaired tumor development. CRISPR/Cas9-mediated knockout of *Ire1α*, *Xbp1*, or *Perk* led to severely reduced growth of INS-1 xenografts. Furthermore, within 24-48 hours of administration, small molecule inhibitors of IRE1α (KIRA8) or PERK (GSK-PKI) halted cell-cycle progression and induced apoptosis (as measured by Caspase-3 cleavage) in INS-1 xenografts. *In vivo*, we saw evidence that inhibiting one arm of the UPR (e.g. IRE1α), led to compensatory hyperactivation of the other (PERK), and vice versa. For example, inhibiting IRE1α with KIRA8 led to transcriptional upregulation of PERK-associated ER stress markers (*Bip, Ire1α*) and apoptotic outputs (*Txnip*, *Bim*). Similarly, PERK inhibition with GSK-PKI caused a significant increase in IRE1α's adaptive (*Xbp1s*) and apoptotic outputs (RIDD as measured by *Ins1* and *Ins2* mRNA decay).

By artificially inducing ER stress in cultured INS-1 cells, we were able to recapitulate and dissect the cytotoxic effects of KIRA8 and GSK-PKI seen *in vivo* in the PanNETs. In this controlled setting, inhibiting IRE1α leads to higher sustained activation of PERK and its pro-apoptotic target CHOP. Inversely, PERK inhibition results in IRE1α hyperactivation. In both cases, this leads to loss of an adaptive arm of the UPR, worsening

ER stress, and shifts the ER stress burden to the remaining branch, triggering its apoptotic (Terminal) program. Given that targeting one arm of the UPR both reduces its adaptive outputs and leads to compensatory pro-apoptotic activation of the other arm, further studies will be needed to understand the individual contributions of these effects on PanNET growth.

Ultimately, the most important aspect of pharmacologically targeting the UPR is its translational potential. To determine whether our results generalize to other PanNET models, we tested KIRA8 and GSK-PKI in the well-characterized transgenic RIP-Tag2 model. In use for over 20 years, this model has predicted the clinical efficacy of several compounds that have gone on to FDA approval for pancreatic neuroendocrine tumors, including everolimus and sunitinib. Furthermore, in comparison to the INS-1 xenograft model, RIP-Tag2 tumors arise directly from endogenous pancreatic β-cells and therefore develop in their natural environment. Although both KIRA8 and GSK-PKI are effective at reducing tumor burden in this model, the stark difference in their pancreatic toxicities sets them apart. Within two weeks, daily GSK-PKI administration to wild-type C57BL/6 mice severely damaged and reduced pancreatic mass to approximately 50% that of vehicle-treated controls; similar results were previously obtained using oral administration of this PERK inhibitor in CD-1 mice (Atkins et al., 2013), mirroring the effects of deletion or mutation of PERK in pancreatic β-cells (Delepine et al., 2000).

Because genetic deletion of either *Perk* or *Ire1α* can lead to β-cell dysfunction and apoptosis, it had been widely assumed that KIRAs would have similar toxicities to PERK inhibitors. Strikingly, commensurate with its limited effects on overall animal health, KIRA8 administration had no noticeable effect on pancreatic mass or histology in wild-

type C57BL/6 or RIP-Tag2 mice. Likewise, inhibiting IRE1α with KIRA8 (or related compound KIRA6) was well tolerated and preserved pancreatic β-cell health in multiple diabetes models (Ghosh et al., 2014; Morita et al., 2017). Therefore, we tested whether KIRA8 would be effective in controlling PanNET growth after tumors had developed in RIP-Tag2 mice. We found that daily KIRA8 administration to tumor-bearing 12-week-old RIP-Tag2 mice not only reduced tumor growth but also increased survival time by over 2-fold. As such, IRE1α emerges as a more attractive therapeutic target than PERK. Regardless, more studies will need to be done to understand the long-term effects of IRE1α inhibition.

Other facets of our data hint at alternative strategies for targeting IRE1α in PanNETs. For one, KIRA8 had a more dramatic effect on tumor burden in the RIP-Tag2 model than in the INS-1 xenograft model. The pancreata of KIRA8-treated mice much more closely resemble those of wild-type control mice with no grossly visible pancreatic tumors; in contrast, the pancreata of vehicle-treated mice are filled with macroscopic tumors. The difference in immunocompetence between NSG (xenograft) and C57BL/6 mice (RIP-Tag2 background) may be one decisive factor. For example, recent reports suggest that targeting the IRE1α-XBP1 axis may engage a two-pronged attack that restrains malignant cells while simultaneously eliciting concomitant antitumor immunity through mechanisms involving dendritic cell antigen presentation (Cubillos-Ruiz et al., 2015). The recent explosion in immunotherapy suggests that the immune system has a more complex and widespread role in cancer than initially appreciated, and manipulating the UPR may enhance this approach (Cubillos-Ruiz et al., 2017; Cubillos-Ruiz and Glimcher, 2016).

Together, our findings reveal many crucial aspects of studying and targeting the UPR in PanNETs. Both the intrinsic secretory nature of PanNETs and their surrounding environments contribute to their level of ER stress, forcing them to lean on the Adaptive UPR for survival. Consequently, modulation of IRE1α or PERK activity shifts tumor cells away from the Adaptive UPR, resulting in growth arrest and apoptosis. Similarly, low baseline levels of ER stress in healthy tissues reduce their dependency on UPR signaling and likely shield them from toxic side effects, particularly under administration of IRE1α inhibitors like KIRA8. The seemingly paradoxical observation that IRE1α inhibition preserves beta cell mass in diabetes models (Akita, NOD) (Ghosh et al., 2014; Morita et al., 2017) but reduces beta cell-derived tumors likely results from the intrinsic proliferative capacities for the two cell types: normal pancreatic beta cells are generally post-mitotic and have a very low proliferation rate. Ultimately, optimization of current inhibitors, exploration of combination therapies, and enhancement of UPR activators will diversify our treatment strategies for targeting the UPR. Moreover, because this approach is not dependent on the presence of a somatic mutation in a UPR component, it may have benefits in many other solid tumors where ER stress is documented.

Author Contributions

Conceptualization, P.C.M., J.Y.Q., S.A.O., and F.R.P.; Methodology, P.C.M., J.Y.Q., A.H., and S.A.O.; Validation, P.C.M. and J.Y.Q.; Formal Analysis, P.C.M., J.Y.Q., and M.T.; Investigation, P.C.M., J.Y.Q., M.T., P.J.T., R.G., and R.E.W.; Resources, G.E.K., M.J.G., B.J.B., and D.J.M; Writing – Original Draft, J.Y.Q. and S.A.O.; Writing – Review & Editing, P.C.M., J.Y.Q., F.R.P., and S.A.O.; Visualization, P.C.M., J.Y.Q.; Supervision, S.A.O.; Funding Acquisition, S.A.O. and F.R.P.

Acknowledgements

We thank the UCSF Diabetes Center and the UCSF Brain Tumor Research Center (BTRC) for tissue processing and sectioning; the Tlsty Lab for NSG mice, immunohistochemistry protocols, and use of machines; Dr. Rushika Perera for technical assistance with RIP-Tag2 tumor analysis; the Cyster lab for use of their microscope; the Goga and Maltepe Labs for use of incubators; the Goga and Debnath Labs for antibodies; the Hebrok Lab for help with islet histology; Dr. Ed Roberts for help with mouse procedures; Vinh Nguyen for assistance with pancreas dissociation; Lita and Lorna Espinoza for lab maintenance; Elva Kogl, Dayi Su, and Veronica Kuiper for mouse care; Matthias Hebrok, Andrei Goga, and Oakes and Papa Lab members for discussions. The work was supported by grants; American Cancer Society Research Scholar Award (S.A.O.); Harrington Discovery Institute Scholar-Innovator Award (S.A.O. and F.R.P.); UCSF and Onyx Oncology Innovation Alliance (S.A.O. and F.R.P.); Alfred P. Sloan Foundation (D.J.M.); Camille and Henry Dreyfus Foundation (D.J.M.); American Association of Cancer Research (S.A.O.); National Science Foundation (J.Y.Q.); NIH/NCI

Brain Tumor SPORE (UCSF BTRC) the P50 CA097257 NIH/NCI Brain Tumor SPORE Grant. R01CA219815 (S.A.O.), R01EY027810 (S.A.O.; F.R.P.), U01DK108332 (S.A.O.), T32CA177555 (S.A.O.)

CONFLICT OF INTEREST

D.J.M., B.J.B., F.R. P, and S.A.O. are founders, equity holders, and consultants for OptiKIRA, LLC (Cleveland, OH), a biotech company focused on treating ER-stress induced retinal degeneration.

References

Aragon, T., van Anken, E., Pincus, D., Serafimova, I.M., Korennykh, A.V., Rubio, C.A., and Walter, P. (2009). Messenger RNA targeting to endoplasmic reticulum stress signalling sites. Nature *457*, 736-740.

Asfari, M., Janjic, D., Meda, P., Li, G., Halban, P.A., and Wollheim, C.B. (1992). Establishment of 2-mercaptoethanol-dependent differentiated insulin-secreting cell lines. Endocrinology *130*, 167-178.

Atkins, C., Liu, Q., Minthorn, E., Zhang, S.Y., Figueroa, D.J., Moss, K., Stanley, T.B., Sanders, B., Goetz, A., Gaul, N.*, et al.* (2013). Characterization of a novel PERK kinase inhibitor with antitumor and antiangiogenic activity. Cancer Res *73*, 1993-2002.

Auf, G., Jabouille, A., Guerit, S., Pineau, R., Delugin, M., Bouchecareilh, M., Magnin, N., Favereaux, A., Maitre, M., Gaiser, T.*, et al.* (2010). Inositol-requiring enzyme 1alpha is a key regulator of angiogenesis and invasion in malignant glioma. Proc Natl Acad Sci U S A *107*, 15553-15558.

Babu, V., Paul, N., and Yu, R. (2013). Animal models and cell lines of pancreatic neuroendocrine tumors. Pancreas *42*, 912-923.

Baudin, E., Gigliotti, A., Ducreux, M., Ropers, J., Comoy, E., Sabourin, J.C., Bidart, J.M., Cailleux, A.F., Bonacci, R., Ruffie, P.*, et al.* (1998). Neuron-specific enolase and chromogranin A as markers of neuroendocrine tumours. Br J Cancer *78*, 1102-1107.

Bergers, G., Javaherian, K., Lo, K.M., Folkman, J., and Hanahan, D. (1999). Effects of angiogenesis inhibitors on multistage carcinogenesis in mice. Science *284*, 808-812.

Bobrovnikova-Marjon, E., Grigoriadou, C., Pytel, D., Zhang, F., Ye, J., Koumenis, C., Cavener, D., and Diehl, J.A. (2010). PERK promotes cancer cell proliferation and tumor growth by limiting oxidative DNA damage. Oncogene *29*, 3881-3895.

Carrasco, D.R., Sukhdeo, K., Protopopova, M., Sinha, R., Enos, M., Carrasco, D.E., Zheng, M., Mani, M., Henderson, J., Pinkus, G.S.*, et al.* (2007). The differentiation and stress response factor XBP-1 drives multiple myeloma pathogenesis. Cancer Cell *11*, 349-360.

Chen, X., Ding, Y., Liu, C.G., Mikhail, S., and Yang, C.S. (2002). Overexpression of glucose-regulated protein 94 (Grp94) in esophageal adenocarcinomas of a rat surgical model and humans. Carcinogenesis *23*, 123-130.

Cives, M., and Strosberg, J. (2017). Radionuclide Therapy for Neuroendocrine Tumors. Curr Oncol Rep *19*, 9.

Credle, J.J., Finer-Moore, J.S., Papa, F.R., Stroud, R.M., and Walter, P. (2005). On the mechanism of sensing unfolded protein in the endoplasmic reticulum. Proc Natl Acad Sci U S A *102*, 18773-18784.

Cubillos-Ruiz, J.R., Bettigole, S.E., and Glimcher, L.H. (2017). Tumorigenic and Immunosuppressive Effects of Endoplasmic Reticulum Stress in Cancer. Cell *168*, 692-706.

Cubillos-Ruiz, J.R., and Glimcher, L.H. (2016). Targeting abnormal ER stress responses in tumors: A new approach to cancer immunotherapy. Oncoimmunology *5*, e1098802.

Cubillos-Ruiz, J.R., Silberman, P.C., Rutkowski, M.R., Chopra, S., Perales-Puchalt, A., Song, M., Zhang, S., Bettigole, S.E., Gupta, D., Holcomb, K.*, et al.* (2015). ER Stress Sensor XBP1 Controls Anti-tumor Immunity by Disrupting Dendritic Cell Homeostasis. Cell *161*, 1527-1538.

Cui, W., Li, J., Ron, D., and Sha, B. (2011). The structure of the PERK kinase domain suggests the mechanism for its activation. Acta Crystallogr D Biol Crystallogr *67*, 423-428.

Delepine, M., Nicolino, M., Barrett, T., Golamaully, M., Lathrop, G.M., and Julier, C. (2000). EIF2AK3, encoding translation initiation factor 2-alpha kinase 3, is mutated in patients with Wolcott-Rallison syndrome. Nat Genet *25*, 406-409.

Feldman, H.C., Tong, M., Wang, L., Meza-Acevedo, R., Gobillot, T.A., Lebedev, I., Gliedt, M.J., Hari, S.B., Mitra, A.K., Backes, B.J.*, et al.* (2016). Structural and Functional Analysis of the Allosteric Inhibition of IRE1alpha with ATP-Competitive Ligands. ACS Chem Biol *11*, 2195-2205.

Fernandez, P.M., Tabbara, S.O., Jacobs, L.K., Manning, F.C., Tsangaris, T.N., Schwartz, A.M., Kennedy, K.A., and Patierno, S.R. (2000). Overexpression of the glucose-regulated stress gene GRP78 in malignant but not benign human breast lesions. Breast Cancer Res Treat *59*, 15-26.

Gardner, B.M., and Walter, P. (2011). Unfolded proteins are Ire1-activating ligands that directly induce the unfolded protein response. Science *333*, 1891-1894.

Ghosh, R., Wang, L., Wang, E.S., Perera, B.G., Igbaria, A., Morita, S., Prado, K., Thamsen, M., Caswell, D., Macias, H.*, et al.* (2014). Allosteric Inhibition of the IRE1alpha RNase Preserves Cell Viability and Function during Endoplasmic Reticulum Stress. Cell *158*, 534-548.

Han, D., Lerner, A.G., Vande Walle, L., Upton, J.P., Xu, W., Hagen, A., Backes, B.J., Oakes, S.A., and Papa, F.R. (2009). IRE1alpha kinase activation modes control alternate endoribonuclease outputs to determine divergent cell fates. Cell *138*, 562-575.

Hanahan, D. (1985). Heritable formation of pancreatic beta-cell tumours in transgenic mice expressing recombinant insulin/simian virus 40 oncogenes. Nature *315*, 115-122.

Harding, H.P., Zhang, Y., Bertolotti, A., Zeng, H., and Ron, D. (2000). Perk is essential for translational regulation and cell survival during the unfolded protein response. Mol Cell *5*, 897-904.

Harding, H.P., Zhang, Y., and Ron, D. (1999). Protein translation and folding are coupled by an endoplasmic-reticulum-resident kinase. Nature *397*, 271-274.

Harrington, P.E., Biswas, K., Malwitz, D., Tasker, A.S., Mohr, C., Andrews, K.L., Dellamaggiore, K., Kendall, R., Beckmann, H., Jaeckel, P*., et al.* (2015). Unfolded Protein Response in Cancer: IRE1alpha Inhibition by Selective Kinase Ligands Does Not Impair Tumor Cell Viability. ACS Med Chem Lett *6*, 68-72.

Hassler, J.R., Scheuner, D.L., Wang, S., Han, J., Kodali, V.K., Li, P., Nguyen, J., George, J.S., Davis, C., Wu, S.P*., et al.* (2015). The IRE1alpha/XBP1s Pathway Is Essential for the Glucose Response and Protection of beta Cells. PLoS Biol *13*, e1002277.

Hetz, C., Chevet, E., and Oakes, S.A. (2015). Proteostasis control by the unfolded protein response. Nat Cell Biol *17*, 829-838.

Hollien, J., Lin, J.H., Li, H., Stevens, N., Walter, P., and Weissman, J.S. (2009). Regulated Ire1-dependent decay of messenger RNAs in mammalian cells. J Cell Biol *186*, 323-331.

Jamora, C., Dennert, G., and Lee, A.S. (1996). Inhibition of tumor progression by suppression of stress protein GRP78/BiP induction in fibrosarcoma B/C10ME. Proc Natl Acad Sci U S A *93*, 7690-7694.

Kosmaczewski, S.G., Edwards, T.J., Han, S.M., Eckwahl, M.J., Meyer, B.I., Peach, S., Hesselberth, J.R., Wolin, S.L., and Hammarlund, M. (2014). The RtcB RNA ligase is an essential component of the metazoan unfolded protein response. EMBO Rep *15*, 1278-1285.

Koumenis, C. (2006). ER stress, hypoxia tolerance and tumor progression. Curr Mol Med *6*, 55-69.

Lee, A.H., Heidtman, K., Hotamisligil, G.S., and Glimcher, L.H. (2011). Dual and opposing roles of the unfolded protein response regulated by IRE1alpha and XBP1 in proinsulin processing and insulin secretion. Proc Natl Acad Sci U S A *108*, 8885-8890.

Lee, A.H., Iwakoshi, N.N., and Glimcher, L.H. (2003). XBP-1 regulates a subset of endoplasmic reticulum resident chaperone genes in the unfolded protein response. Mol Cell Biol *23*, 7448-7459.

Lee, A.S., and Hendershot, L.M. (2006). ER stress and cancer. Cancer Biol Ther *5*, 721-722.

Lerner, A.G., Upton, J.P., Praveen, P.V., Ghosh, R., Nakagawa, Y., Igbaria, A., Shen, S., Nguyen, V., Backes, B.J., Heiman, M.*, et al.* (2012). IRE1alpha induces thioredoxin-interacting protein to activate the NLRP3 inflammasome and promote programmed cell death under irremediable ER stress. Cell Metab *16*, 250-264.

Lu, Y., Liang, F.X., and Wang, X. (2014). A synthetic biology approach identifies the mammalian UPR RNA ligase RtcB. Mol Cell *55*, 758-770.

Luo, S., Baumeister, P., Yang, S., Abcouwer, S.F., and Lee, A.S. (2003). Induction of Grp78/BiP by translational block: activation of the Grp78 promoter by ATF4 through and upstream ATF/CRE site independent of the endoplasmic reticulum stress elements. J Biol Chem *278*, 37375-37385.

Ma, Y., and Hendershot, L.M. (2004). The role of the unfolded protein response in tumour development: friend or foe? Nat Rev Cancer *4*, 966-977.

Marciniak, S.J., Yun, C.Y., Oyadomari, S., Novoa, I., Zhang, Y., Jungreis, R., Nagata, K., Harding, H.P., and Ron, D. (2004). CHOP induces death by promoting protein synthesis and oxidation in the stressed endoplasmic reticulum. Genes Dev *18*, 3066-3077.

McCracken, A.A., and Brodsky, J.L. (2003). Evolving questions and paradigm shifts in endoplasmic-reticulum-associated degradation (ERAD). Bioessays *25*, 868-877.

McCullough, K.D., Martindale, J.L., Klotz, L.O., Aw, T.Y., and Holbrook, N.J. (2001). Gadd153 sensitizes cells to endoplasmic reticulum stress by down-regulating Bcl2 and perturbing the cellular redox state. Mol Cell Biol *21*, 1249-1259.

Metz, D.C., and Jensen, R.T. (2008). Gastrointestinal neuroendocrine tumors: pancreatic endocrine tumors. Gastroenterology *135*, 1469-1492.

Meusser, B., Hirsch, C., Jarosch, E., and Sommer, T. (2005). ERAD: the long road to destruction. Nat Cell Biol *7*, 766-772.

Moenner, M., Pluquet, O., Bouchecareilh, M., and Chevet, E. (2007). Integrated endoplasmic reticulum stress responses in cancer. Cancer Res *67*, 10631-10634.

Morita, S., Villalta, S.A., Feldman, H.C., Register, A.C., Rosenthal, W., Hoffmann-Petersen, I.T., Mehdizadeh, M., Ghosh, R., Wang, L., Colon-Negron, K.*, et al.* (2017). Targeting ABL-IRE1alpha Signaling Spares ER-Stressed Pancreatic beta Cells to Reverse Autoimmune Diabetes. Cell Metab *25*, 883-897 e888.

Nobels, F.R., Kwekkeboom, D.J., Bouillon, R., and Lamberts, S.W. (1998). Chromogranin A: its clinical value as marker of neuroendocrine tumours. Eur J Clin Invest *28*, 431-440.

Oakes, S.A. (2017). Endoplasmic reticulum proteostasis: a key checkpoint in cancer. Am J Physiol Cell Physiol *312*, C93-C102.

Oakes, S.A., and Papa, F.R. (2015). The role of endoplasmic reticulum stress in human pathology. Annu Rev Pathol *10*, 173-194.

Oberg, K., and Eriksson, B. (2005). Endocrine tumours of the pancreas. Best Pract Res Clin Gastroenterol *19*, 753-781.

Park, H.R., Tomida, A., Sato, S., Tsukumo, Y., Yun, J., Yamori, T., Hayakawa, Y., Tsuruo, T., and Shin-ya, K. (2004). Effect on tumor cells of blocking survival response to glucose deprivation. J Natl Cancer Inst *96*, 1300-1310.

Pirker, R.A., Pont, J., Pohnl, R., Schutz, W., Griesmacher, A., and Muller, M.M. (1998). Usefulness of chromogranin A as a marker for detection of relapses of carcinoid tumours. Clin Chem Lab Med *36*, 837-840.

Puthalakath, H., O'Reilly, L.A., Gunn, P., Lee, L., Kelly, P.N., Huntington, N.D., Hughes, P.D., Michalak, E.M., McKimm-Breschkin, J., Motoyama, N.*, et al.* (2007). ER stress triggers apoptosis by activating BH3-only protein Bim. Cell *129*, 1337-1349.

Raymond, E., Dahan, L., Raoul, J.L., Bang, Y.J., Borbath, I., Lombard-Bohas, C., Valle, J., Metrakos, P., Smith, D., Vinik, A.*, et al.* (2011). Sunitinib malate for the treatment of pancreatic neuroendocrine tumors. N Engl J Med *364*, 501-513.

Rojas-Rivera, D., Delvaeye, T., Roelandt, R., Nerinckx, W., Augustyns, K., Vandenabeele, P., and Bertrand, M.J.M. (2017). When PERK inhibitors turn out to be new potent RIPK1 inhibitors: critical issues on the specificity and use of GSK2606414 and GSK2656157. Cell Death Differ *24*, 1100-1110.

Romero-Ramirez, L., Cao, H., Nelson, D., Hammond, E., Lee, A.H., Yoshida, H., Mori, K., Glimcher, L.H., Denko, N.C., Giaccia, A.J.*, et al.* (2004). XBP1 is essential for survival under hypoxic conditions and is required for tumor growth. Cancer Res *64*, 5943-5947
.
Ron, D., and Walter, P. (2007). Signal integration in the endoplasmic reticulum unfolded protein response. Nat Rev Mol Cell Biol *8*, 519-529.

Scheuner, D., and Kaufman, R.J. (2008). The unfolded protein response: a pathway that links insulin demand with beta-cell failure and diabetes. Endocr Rev *29*, 317-333.

Sevier, C.S., and Kaiser, C.A. (2002). Formation and transfer of disulphide bonds in living cells. Nat Rev Mol Cell Biol *3*, 836-847.

Shi, Y., Vattem, K.M., Sood, R., An, J., Liang, J., Stramm, L., and Wek, R.C. (1998). Identification and characterization of pancreatic eukaryotic initiation factor 2 alpha-subunit kinase, PEK, involved in translational control. Mol Cell Biol *18*, 7499-7509.

Shore, G.C., Papa, F.R., and Oakes, S.A. (2011). Signaling cell death from the endoplasmic reticulum stress response. Curr Opin Cell Biol *23*, 143-149.

Shuda, M., Kondoh, N., Imazeki, N., Tanaka, K., Okada, T., Mori, K., Hada, A., Arai, M., Wakatsuki, T., Matsubara, O*., et al.* (2003). Activation of the ATF6, XBP1 and grp78 genes in human hepatocellular carcinoma: a possible involvement of the ER stress pathway in hepatocarcinogenesis. J Hepatol *38*, 605-614.

Smith, M.H., Ploegh, H.L., and Weissman, J.S. (2011). Road to ruin: targeting proteins for degradation in the endoplasmic reticulum. Science *334*, 1086-1090.

Song, M.S., Park, Y.K., Lee, J.H., and Park, K. (2001). Induction of glucose-regulated protein 78 by chronic hypoxia in human gastric tumor cells through a protein kinase C-epsilon/ERK/AP-1 signaling cascade. Cancer Res *61*, 8322-8330.

Tsuru, A., Imai, Y., Saito, M., and Kohno, K. (2016). Novel mechanism of enhancing IRE1alpha-XBP1 signalling via the PERK-ATF4 pathway. Sci Rep *6*, 24217.

Tu, B.P., and Weissman, J.S. (2004). Oxidative protein folding in eukaryotes: mechanisms and consequences. J Cell Biol *164*, 341-346.

Upton, J.P., Wang, L., Han, D., Wang, E.S., Huskey, N.E., Lim, L., Truitt, M., McManus, M.T., Ruggero, D., Goga, A*., et al.* (2012). IRE1alpha cleaves select microRNAs during ER stress to derepress translation of proapoptotic Caspase-2. Science *338*, 818-822.

van der Zwan, J.M., Trama, A., Otter, R., Larranaga, N., Tavilla, A., Marcos-Gragera, R., Dei Tos, A.P., Baudin, E., Poston, G., Links, T*., et al.* (2013). Rare neuroendocrine tumours: results of the surveillance of rare cancers in Europe project. Eur J Cancer *49*, 2565-2578.

Yao, J.C., Hassan, M., Phan, A., Dagohoy, C., Leary, C., Mares, J.E., Abdalla, E.K., Fleming, J.B., Vauthey, J.N., Rashid, A*., et al.* (2008). One hundred years after "carcinoid": epidemiology of and prognostic factors for neuroendocrine tumors in 35,825 cases in the United States. J Clin Oncol *26*, 3063-3072.

Yao, J.C., Shah, M.H., Ito, T., Bohas, C.L., Wolin, E.M., Van Cutsem, E., Hobday, T.J., Okusaka, T., Capdevila, J., de Vries, E.G*., et al.* (2011). Everolimus for advanced pancreatic neuroendocrine tumors. N Engl J Med *364*, 514-523.

Young, S.K., and Wek, R.C. (2016). Upstream Open Reading Frames Differentially Regulate Gene-specific Translation in the Integrated Stress Response. J Biol Chem *291*, 16927-16935.

Zhou, J., Liu, C.Y., Back, S.H., Clark, R.L., Peisach, D., Xu, Z., and Kaufman, R.J. (2006). The crystal structure of human IRE1 luminal domain reveals a conserved dimerization

interface required for activation of the unfolded protein response. Proc Natl Acad Sci U S A *103*, 14343-14348.

Figure Legends

Figure 1. PanNETs show evidence of ER stress and UPR activation.

(A) In response to the accumulation of misfolded proteins in the ER, IRE1α and PERK homodimerize and signal an adaptive stress response through splicing of *Xbp1* and phosphorylation of eIF2α, respectively. However, under sustained ER stress these pathways promote apoptosis through regulated Ire1α-dependent decay (RIDD) and upregulation of the pro-apoptotic factor CHOP.

(B-C) Representative (B) H&E and (C) BiP/GRP78 IHC on normal pancreas and primary human PanNET. Star indicates islet of Langerhans (scale bars, 50 μm).

(D-E) (D) Percent *XBP1* splicing and (E) relative *ATF4* mRNA expression from normal human pancreas and four primary human PanNETs.

(F) PanNET xenograft experimental setup. 5 million INS-1 cells (INS-1 control vs. transgenic variant) injected subcutaneously in bilateral flanks of NSG mice. INS-1 tumors become palpable by ~10 days, and mice are sacrificed for tumor endpoint at 4 weeks post-injection.

(G-K) IHC of human PanNETs and INS-1 mouse xenografts stained with the indicated antibodies (CgA=chromogranin A, SPH=synaptophysin; scale bars, 50 μm).

(L) INS-1 cells were grown in tissue culture (*in vitro*) or as xenografts (*in vivo*) in NSG mice for 2 or 3 weeks. Three unique replicates of each condition were harvested and analyzed by immunoblotting with the indicated antibodies.

See also Figure S1

Figure 2. Manipulation of IRE1α adaptive vs. apoptotic signaling determines growth of INS-1 xenograft tumors

(A) NSG mice were subcutaneously injected with INS-1 (vector) cells or INS-1 cells carrying a doxycycline (Dox)-inducible, Myc-tagged Ire1α gene (INS-1::Ire1α). Mice were fed regular or Dox chow as shown in Figure 1F, and tumors were harvested and weighed after 4 weeks (n ≥ 13; individual values and mean ± SD; unpaired *t* tests).

(B) NSG mice developed INS-1::Vector or INS-1::Ire1α tumors for 14 days before administration of regular or Dox chow for 96 hours. Tumors were harvested and *Ire1α* mRNA levels were quantified (n = 4; mean ± SD; unpaired *t* tests).

(C) Expression of transgenic Myc-tagged IRE1α in tumors treated +/- Dox for 96 hours at 2 weeks post-injection. Immunoblotted with the indicated antibodies; endogenous and Myc-tagged IRE1α species indicated with arrows.

(D) Percent spliced *Xbp1* in INS-1 xenograft tumors treated +/- Dox for 96 hours at 2 weeks post-injection (n ≥ 4; mean ± SD; unpaired t tests).

(E) mRNA levels of *Txnip* at 4 weeks post-injection (n ≥ 13; mean ± SD; unpaired t tests).

(F and G) mRNA levels of (F) *Ins1* and (G) *Ins2* in INS-1 xenograft tumors treated +/- Dox for 96 hours at 2 weeks post-injection (n ≥ 5; mean ± SD; unpaired *t* tests).

(H and I). IHC for (H) Myc and (I) cleaved Caspase-3 in the INS-1 xenograft tumors treated +/- Dox for 96 hours at 2 weeks post-injection (scale bars, 50 μm).

*p<0.05, **p<0.01, ***p<0.001, ****p<0.0001, *****p<0.00001 for (A), (B) and (D-G)

See also Figure S2

Figure 3. CRISPR/Cas9-mediated knockout of IRE1α or PERK pathways dramatically decreases INS-1 tumor burden

(A) Cultured INS-1 control cells and the indicated CRISPR/Cas9 KO clones were treated +/- 0.625 μg/mL Brefeldin A (BFA) for 3 hours prior to harvest to induce ER stress and then immunoblotted with the indicated antibodies.

(B) INS-1 control and the indicated KO lines were subjected to the CellTiter-Glo luminescence-based proliferation assay at 2 and 6 days after seeding. Fold change in luminescence over 96 hours was calculated for each KO line and normalized to INS-1 control (n ≥ 3; mean ± SD; paired *t* test).

(C-E) NSG mice were subcutaneously injected with INS-1 control and one of two unique (C) Ire1α, (D) Xbp1 or (E) Perk KO clones. Resulting tumors were harvested and weighed at 4 weeks post-injection (n ≥ 5; individual values and mean ± SD; unpaired *t* tests).

(F-H). Photos of three representative control and (F) Ire1α, (G) Xbp1 or (H) Perk K tumors from (C-E).

(I) Representative IHC for Ki67 from control and indicated KO tumors at 4 weeks post-injection (n ≥ 4 tumors; scale bars, 50 μm).

(J) Quantification of Ki67 staining in (I) (n ≥ 4; mean ± SD; unpaired *t* tests).

*p<0.05, **p<0.01, ***p<0.001, ****p<0.0001, *****p<0.00001 for (B-E) and (J)

See also Figure S3

Figure 4. Pharmaceutical inhibitors of IRE1α and PERK are effective at inhibiting their kinase targets *in vitro* and *in vivo*

(A) *K*inase *I*nhibiting *R*Nase *A*ttenuator 8 (KIRA8) binds directly to the kinase domain of IRE1α and allosterically inhibits the function of its RNase domain, thereby blocking IRE1α signaling in response to ER stress.

(B) Percent *Xbp1* splicing from cultured INS-1 cells treated concurrently for 20 hours with the indicated concentrations of tunicamycin and KIRA8 (n ≥ 3; mean ± SD; unpaired *t* tests).

(C) *GSK-P*ERK *K*inase *I*nhibitor (GSK-PKI) binds directly to the kinase domain of PERK and blocks signaling in response to ER stress.

(D) Cultured INS-1 cells were treated concurrently for 16 hours with 31.25 nM thapsigargin and the indicated concentrations of GSK-PKI, harvested and immunoblotted with the indicated antibodies.

(E and F) Percentage of cells stained with Annexin V-FITC after five days of treatment with the indicated concentrations of (E) KIRA8 or (F) GSK-PKI (n = 3; mean ± SD; paired *t* tests).

(G) Normalized fold change in luminescence over 96 hours for cells treated with 1 μM KIRA8 or 2 μM GSK (n = 3; mean ± SD; paired *t* tests).

*p<0.05, n.s. = not significant for (B), (E), (F) and (G)

See also Figure S4

Figure 5. Inhibition of Ire1α or Perk leads to compensatory activation of the other arm and increased sensitivity to ER stress-induced apoptosis

(A) Percentage of cultured INS-1 cells stained with Annexin V-FITC after 30 hours of treatment with the indicated combinations of 31.25 nM thapsigargin, 500 nM KIRA8 and 500 nM GSK-PKI (n ≥ 6; mean ± SD; paired *t* tests).

(B) Cultured INS-1 cells were treated for 20 hours with the indicated concentrations of thapsigargin, KIRA8 and GSK-PKI, harvested, and immunoblotted with the indicated antibodies. Both long and short exposures for CHOP are shown. Solid black line indicates excised lane between lanes 3 and 4.

(C) Cultured INS-1 cells were treated concurrently with the indicated combinations of 31.25 nM thapsigargin and 1 μM KIRA8. After 16 hours, cells were placed in thapsigargin-free media while KIRA8 treatment was maintained where indicated. Samples were harvested over the indicated time course and immunoblotted with the indicated antibodies.

(D) Percent *Xbp1* splicing from cells treated as in (B) (n = 3; mean ± SD; paired *t* tests).

*p<0.05, ***p<0.001 for (A) and (D)

See also Figure S5

Figure 6. Pharmacological inhibition of Ire1α or Perk decreases INS-1 tumor size

(A) NSG mice were subcutaneously injected with INS-1 cells and 2 weeks later intraperitoneally injected daily with vehicle or 50 mg/kg KIRA8. Tumors were harvested after 48 hours of vehicle or KIRA8 treatment and subjected to *Xbp1* splicing analysis (n = 4; mean ± SD; unpaired *t* test).

(B) NSG mice were subcutaneously injected with INS-1 cells and 2 weeks later intraperitoneally injected daily with vehicle or 50 mg/kg GSK-PKI. Tumors were harvested

after 48 hours of vehicle or GSK-PKI treatment and immunoblotted with the indicated antibodies.

(C and D) NSG mice were subcutaneously injected with INS-1 cells and administered (C) 30 mg/kg/d KIRA8 or (D) 50 mg/kg/d GSK-PKI. Resulting tumors were harvested and weighed at 3 weeks post-injection (n ≥ 10; individual values and mean ± SD; unpaired *t* test).

(E and F) Photos of three representative vehicle- and (E) KIRA8- or (F) GSK-PKI-treated tumors from (C) and (D), respectively.

**p<0.01, ****p<0.0001 for (A), (C) and (D)

See also Figure S6

Figure 7. KIRA8 and GSK-PKI induce cell-cycle arrest and apoptosis in INS-1 tumors

(A and B) Representative IHC for Ki67 in tumors treated for 48 hours with (A) 50 mg/kg/d KIRA8, (B) 50 mg/kg/d GSK, or the corresponding vehicle (scale bars, 50 μm).

(C and D) Quantitation of Ki67 positive cells from (A) and (B), respectively (n ≥ 4 tumors; mean ± SD; unpaired *t* test).

(E and F) Representative IHC for Cleaved Caspase-3 in tumors from (A) and (B), respectively (scale bars, 50 μm).

(G and H) Quantiation of Cleaved Caspase-3 positive cells from (E) and (F), respectively (n ≥ 4 tumors; mean ± SD; unpaired *t* test).

(I) Levels of the indicated mRNAs from tumors in (A) and (E) (n ≥ 4; mean ± SD; unpaired *t* tests).

(J) Percent *Xbp1* splicing in tumors from (B) and (F) (n = 4; mean ± SD; unpaired *t* test).

(K) mRNA levels of *Ins1* and *Ins2* in tumors from (B) and (F) (n = 4; mean ± SD; unpaired *t* tests).

*p<0.05, **p<0.01, ***p<0.001, ****p<0.0001, *****p<0.00001 for (C), (D) and (G)-(K)

See Also Figure S7

Figure 8. KIRA8 treatment decreases tumor size and prolongs survival in a RIP-Tag2 PanNET model

(A) Timeline of islet tumorigenesis in the RIP-Tag2 model.

(B) Percent *Xbp1* splicing in pancreatic tissue taken from 14-week-old WT and RIP-Tag2 (RT2) C57BL/6 mice (n = 5; mean ± SD; unpaired *t* test).

(C) Tissue from WT and RT2 mice as in (B) harvested and immunoblotted with the indicated antibodies. Low and High phosphorylation states of PERK species are indicated.

(D and E) Representative H&E stains of RT2 pancreata from mice treated with (C) 50 mg/kg/d KIRA8, (D) 50 mg/kg/d GSK-PKI, or the corresponding vehicle beginning at 12 weeks of age and harvested two weeks later (14 days of treatment). Neuroendocrine tissue tumors are outlined in yellow (scale bars, 200 μm).

(F) Percent neuroendocrine tissue area in H&E-stained pancreata from RT2 mice treated with vehicle or KIRA8 as in (C) (n ≥ 7; mean ± SD; unpaired *t* test).

(G) Mass of pancreatic tumors harvested from RT2 mice treated with vehicle or GSK-PKI as in (D) (n ≥ 6; mean ± SD; unpaired *t* test).

(H and I) Representative H&E stains of pancreata from 14-week-old wild-type C57BL/6 mice treated 14 total days with (C) 50 mg/kg/d KIRA8, (D) 50 mg/kg/d GSK-PKI, or the corresponding vehicle (scale bars, 200 μm).

(J) Survival curves of RT2 mice treated with vehicle or 50 mg/kg/d KIRA8 from 12 weeks of age until death (n = 7; individual values; log-rank test).

**p<0.01 for (B), (F), (G) and (J)

See also Figure S8

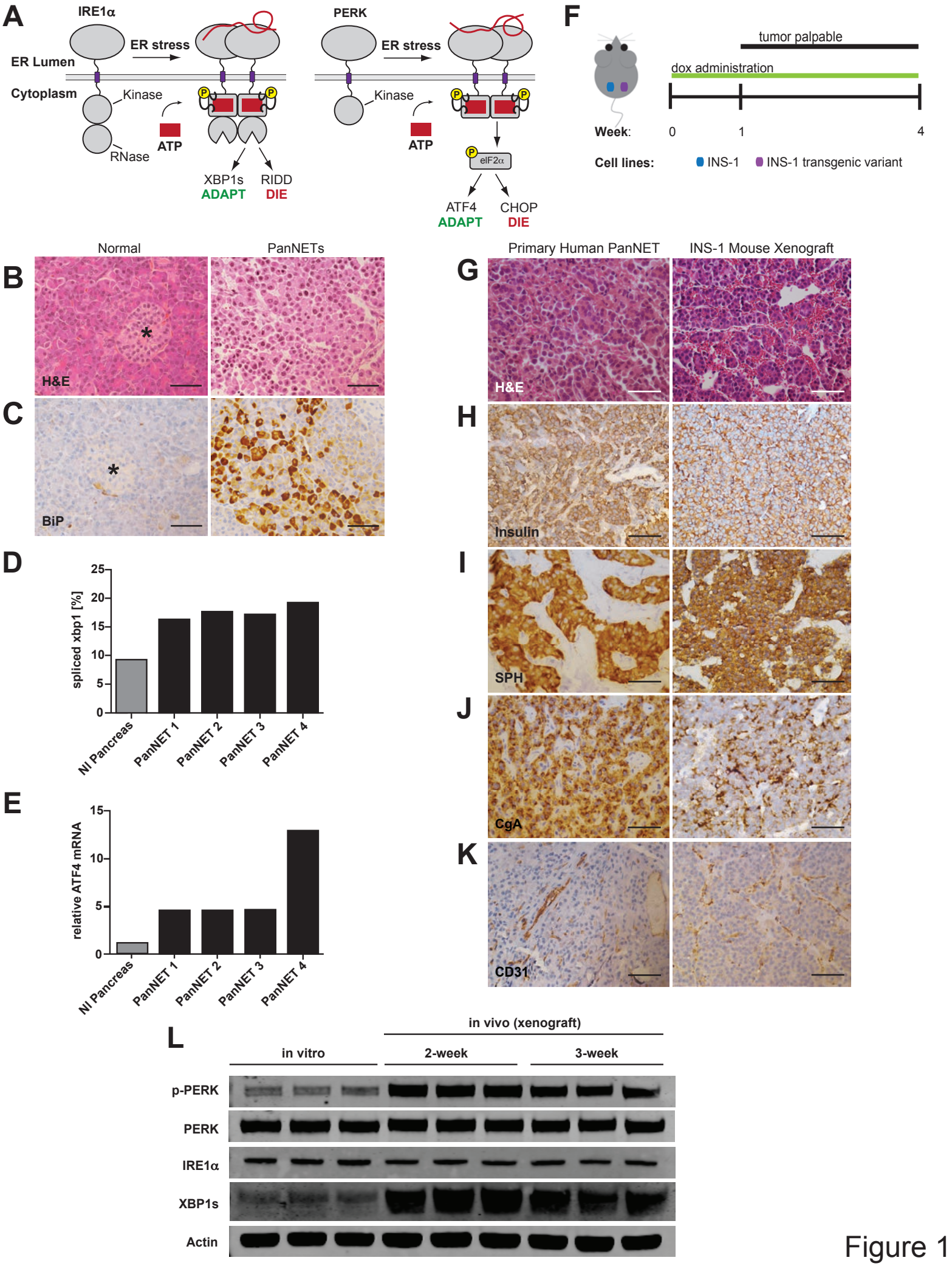
A
IRE1α
ER stress
ER Lumen
Cytoplasm
Kinase
RNase
ATP
XBP1s
ADAPT
RIDD
DIE
PERK
ER stress
Kinase
ATP
eIF2α
ATF4
ADAPT
CHOP
DIE
F
tumor palpable
dox administration
Week:
0
1
4
Cell lines:
INS-1
INS-1 transgenic variant
Normal
PanNETs
B
H&E
C
BiP
D
spliced xbp1 [%]
25
20
15
10
5
0
NI Pancreas
PanNET 1
PanNET 2
PanNET 3
PanNET 4
E
relative ATF4 mRNA
15
10
5
0
NI Pancreas
PanNET 1
PanNET 2
PanNET 3
PanNET 4
Primary Human PanNET
INS-1 Mouse Xenograft
G
H&E
H
Insulin
I
SPH
J
CgA
K
CD31
L
in vivo (xenograft)
in vitro
2-week
3-week
p-PERK
PERK
IRE1α
XBP1s
Actin

Figure 1

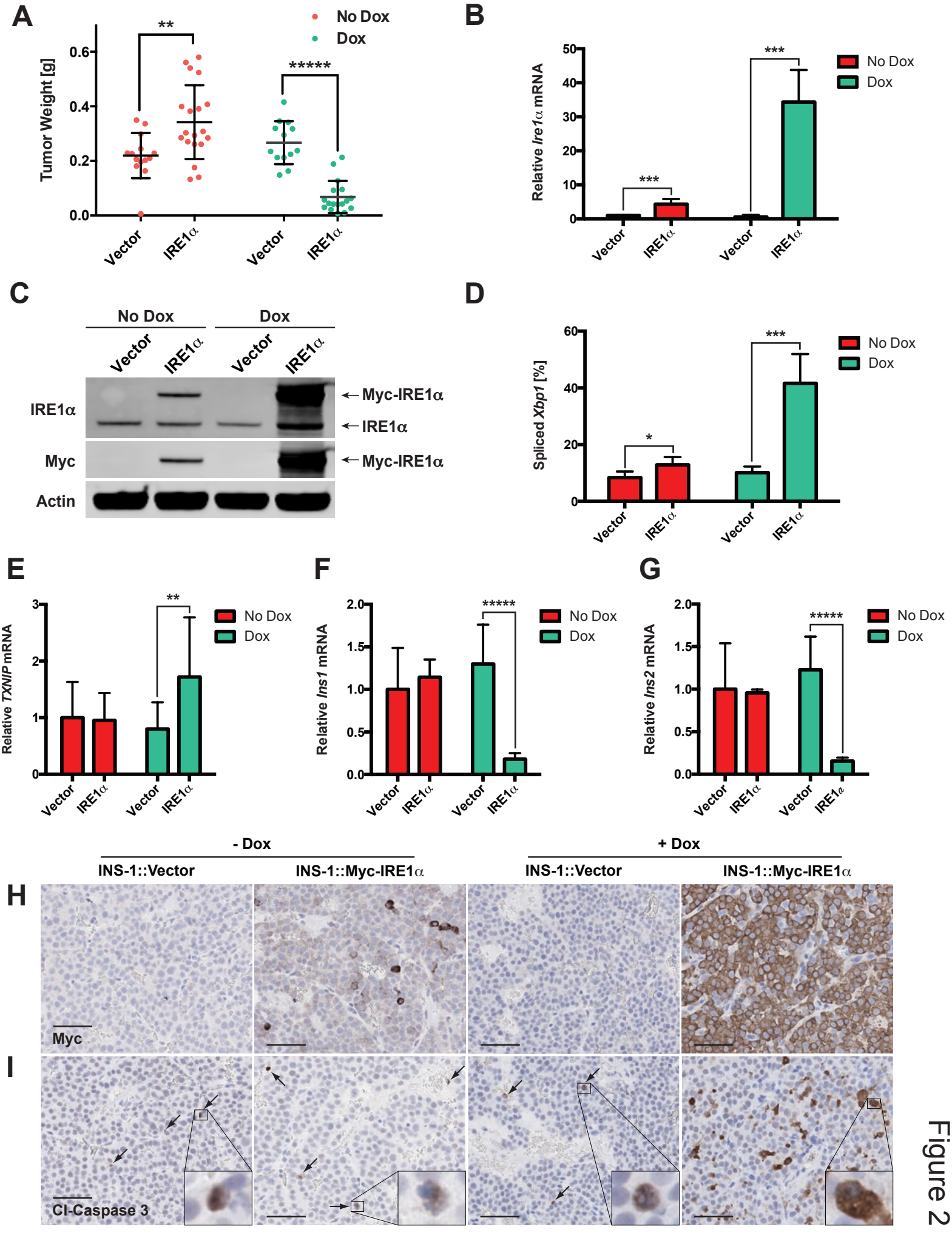
A
No Dox
Dox
Tumor Weight [g]
0.0
0.2
0.4
0.6
**
******
Vector
IRE1α
Vector
IRE1α
B
Relative Ire1α mRNA
0
10
20
30
40
50
***
***
No Dox
Dox
Vector
IRE1α
Vector
IRE1α
C
No Dox
Dox
Vector
IRE1α
Vector
IRE1α
IRE1α
Myc
Actin
←Myc-IRE1α
←IRE1α
←Myc-IRE1α
D
Spliced Xbp1 [%]
0
20
40
60
*
***
No Dox
Dox
Vector
IRE1α
Vector
IRE1α
E
Relative TXNIP mRNA
0
1
2
3
**
No Dox
Dox
Vector
IRE1α
Vector
IRE1α
F
Relative Ins1 mRNA
0.0
0.5
1.0
1.5
2.0
*****
No Dox
Dox
Vector
IRE1α
Vector
IRE1α
G
Relative Ins2 mRNA
0.0
0.5
1.0
1.5
2.0
*****
No Dox
Dox
Vector
IRE1α
Vector
IRE1α
- Dox
+ Dox
INS-1::Vector
INS-1::Myc-IRE1α
INS-1::Vector
INS-1::Myc-IRE1α
H
Myc
I
Cl-Caspase 3

Figure 2

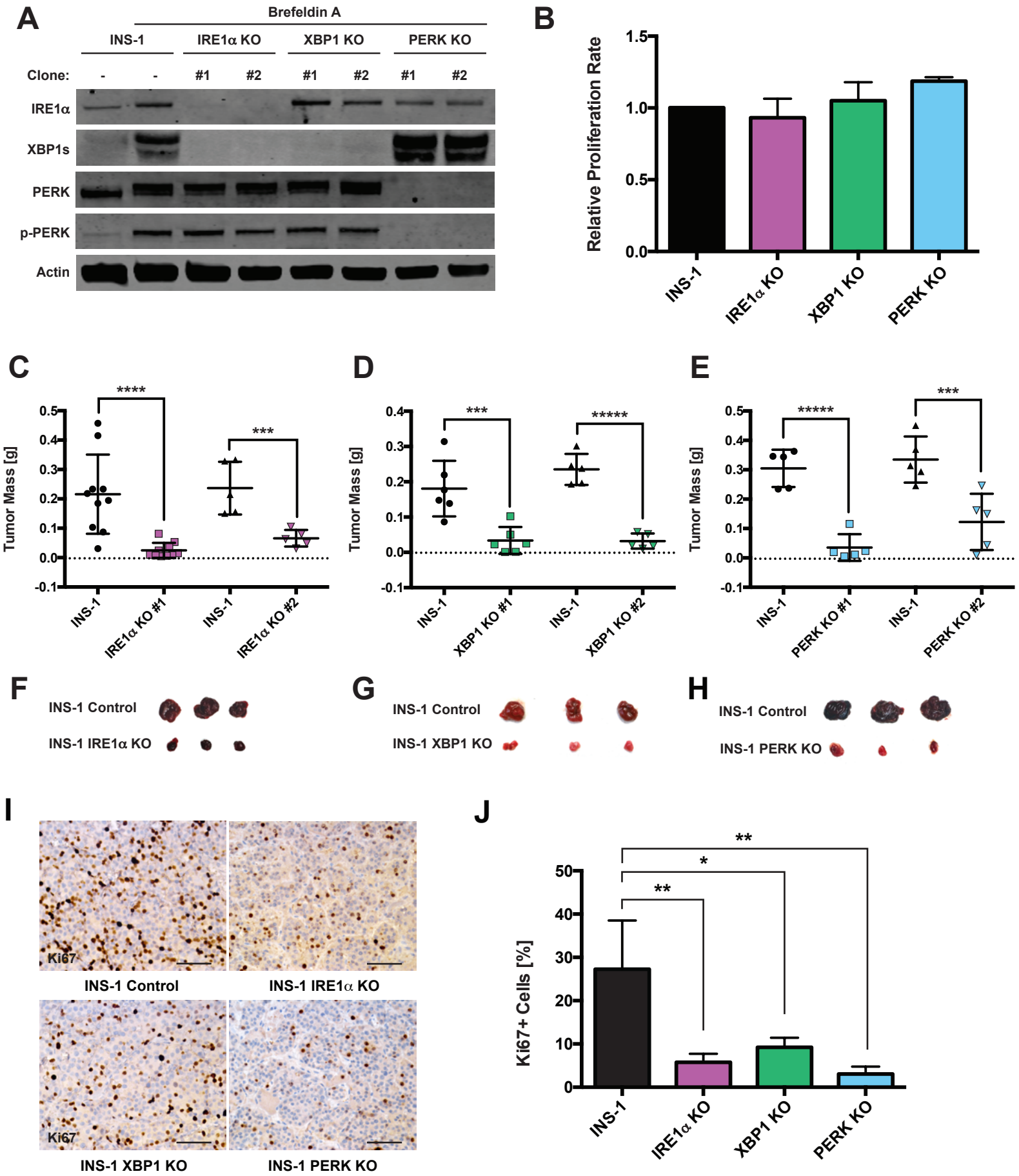
A
Brefeldin A
INS-1
IRE1α KO
XBP1 KO
PERK KO
Clone:
-
-
#1
#2
#1
#2
#1
#2
IRE1α
XBP1s
PERK
p-PERK
Actin
B
Relative Proliferation Rate
1.5
1.0
0.5
0.0
INS-1
IRE1α KO
XBP1 KO
PERK KO
C
Tumor Mass [g]
****
***
INS-1
IRE1α KO #1
INS-1
IRE1α KO #2
D
Tumor Mass [g]
***
*****
INS-1
XBP1 KO #1
INS-1
XBP1 KO #2
E
Tumor Mass [g]
*****
***
INS-1
PERK KO #1
INS-1
PERK KO #2
F
INS-1 Control
INS-1 IRE1α KO
G
INS-1 Control
INS-1 XBP1 KO
H
INS-1 Control
INS-1 PERK KO
I
Ki67
INS-1 Control
INS-1 IRE1α KO
Ki67
INS-1 XBP1 KO
INS-1 PERK KO
J
Ki67+ Cells [%]
**
*
**
50
40
30
20
10
0
INS-1
IRE1α KO
XBP1 KO
PERK KO

Figure 3

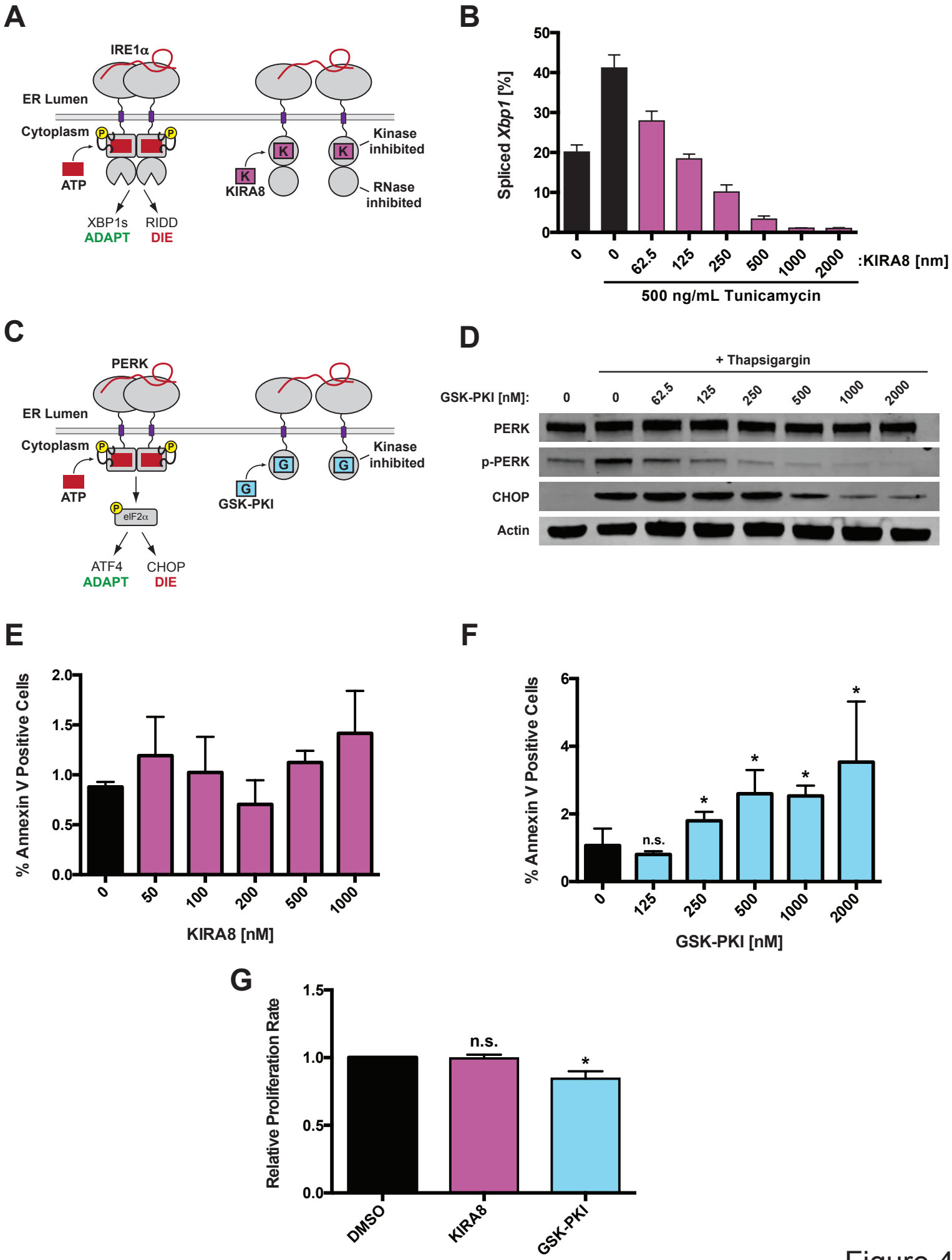
A
IRE1α
ER Lumen
Cytoplasm
ATP
KIRA8
Kinase inhibited
RNase inhibited
XBP1s
ADAPT
RIDD
DIE
B
Spliced Xbp1 [%]
:KIRA8 [nm]
500 ng/mL Tunicamycin
C
PERK
ER Lumen
Cytoplasm
ATP
eIF2α
GSK-PKI
Kinase inhibited
ATF4
ADAPT
CHOP
DIE
D
+ Thapsigargin
GSK-PKI [nM]:
PERK
p-PERK
CHOP
Actin
E
% Annexin V Positive Cells
KIRA8 [nM]
F
% Annexin V Positive Cells
n.s.
GSK-PKI [nM]
G
Relative Proliferation Rate
n.s.
DMSO
KIRA8
GSK-PKI

Figure 4

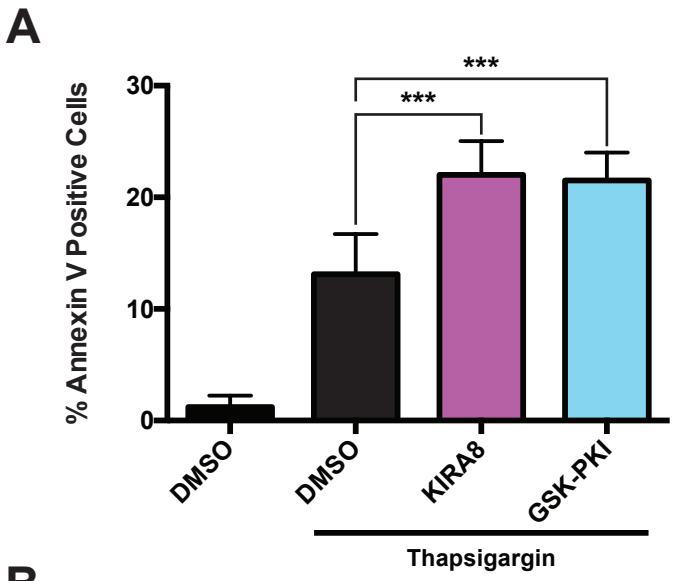
A
% Annexin V Positive Cells
30
20
10
0
***
***
DMSO
DMSO
KIRA8
GSK-PKI
Thapsigargin

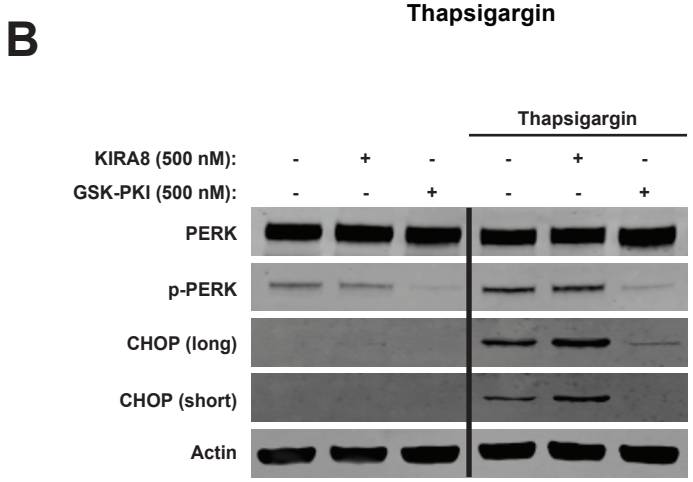
B
Thapsigargin
KIRA8 (500 nM):
GSK-PKI (500 nM):
PERK
p-PERK
CHOP (long)
CHOP (short)
Actin

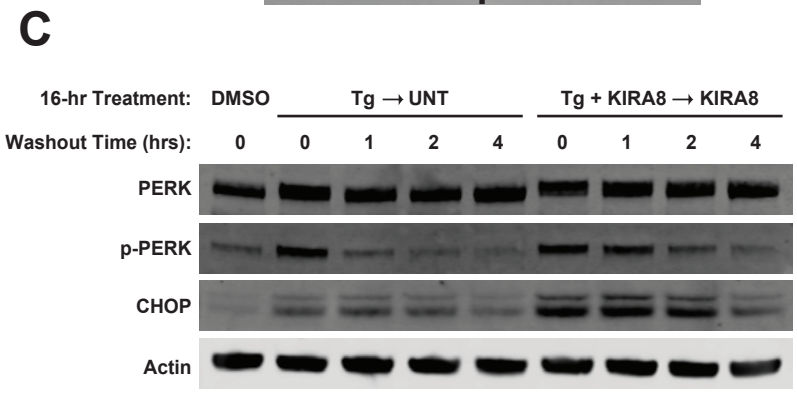
C
16-hr Treatment:
DMSO
Tg → UNT
Tg + KIRA8 → KIRA8
Washout Time (hrs):
0
0
1
2
4
0
1
2
4
PERK
p-PERK
CHOP
Actin

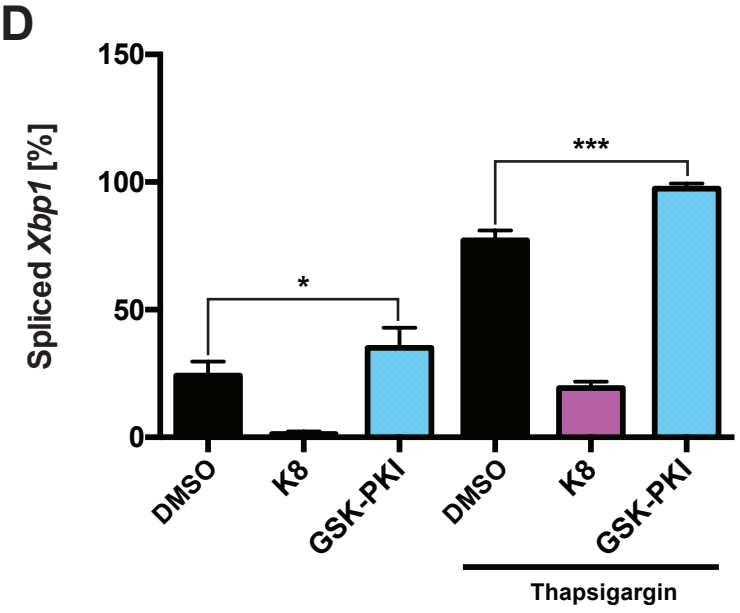
D
Spliced Xbp1 [%]
150
100
50
0
*
***
DMSO
K8
GSK-PKI
DMSO
K8
GSK-PKI
Thapsigargin

Figure 5

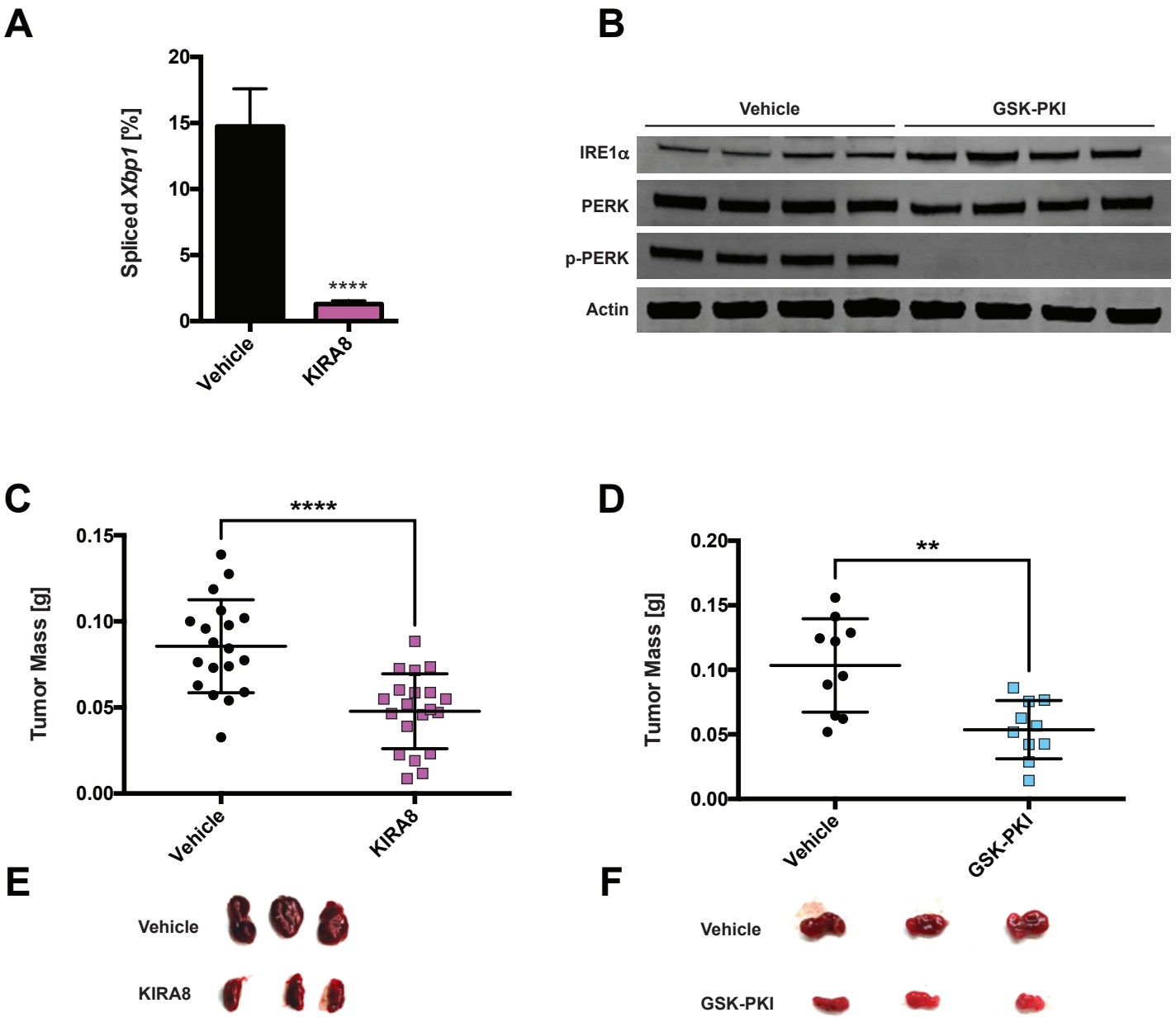
A
Spliced Xbp1 [%]
20
15
10
5
0
****
Vehicle
KIRA8
B
Vehicle
GSK-PKI
IRE1α
PERK
p-PERK
Actin
C
Tumor Mass [g]
0.15
0.10
0.05
0.00
****
Vehicle
KIRA8
D
Tumor Mass [g]
0.20
0.15
0.10
0.05
0.00
**
Vehicle
GSK-PKI
E
Vehicle
KIRA8
F
Vehicle
GSK-PKI

Figure 6

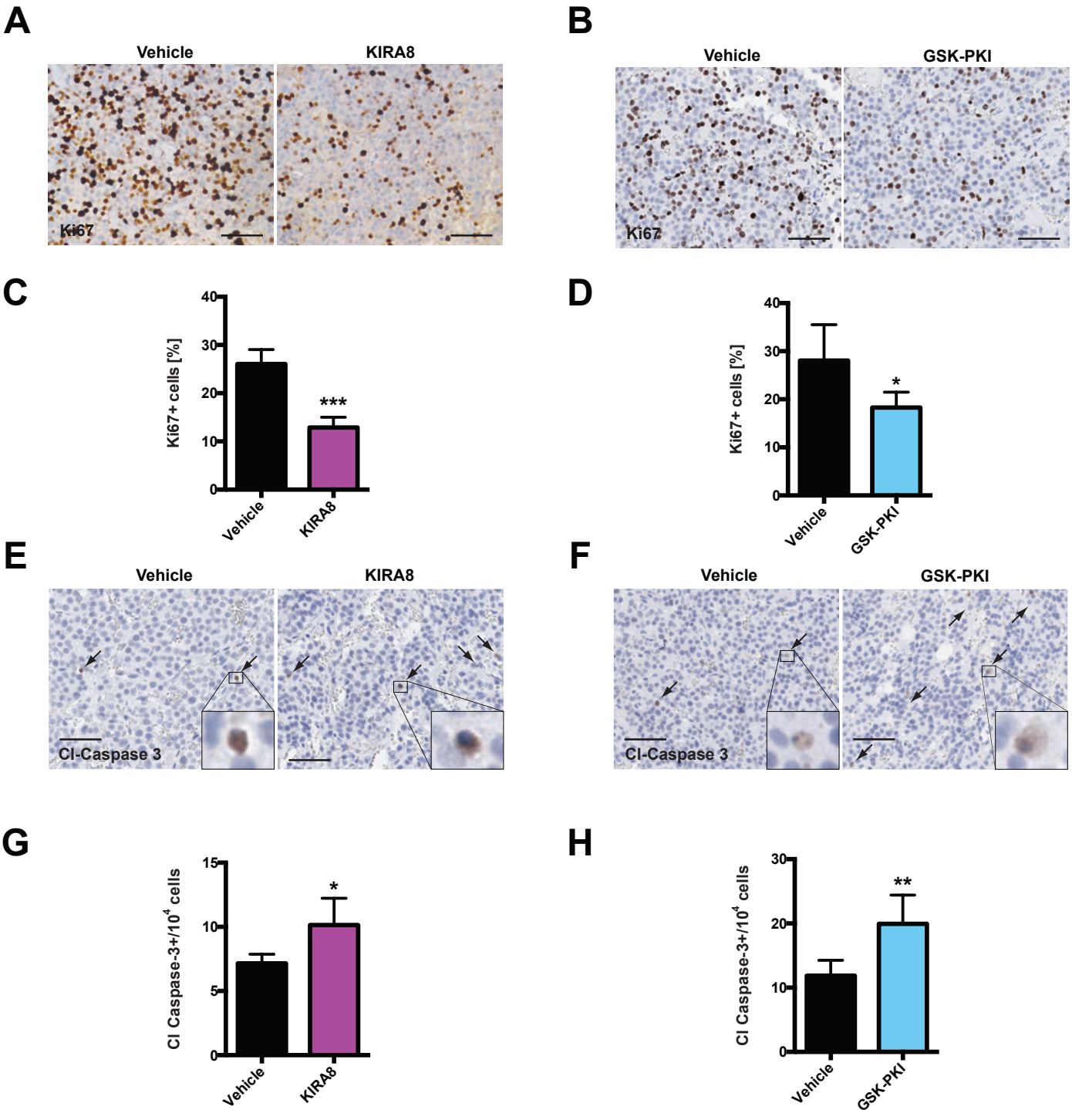
A
Vehicle
KIRA8
Ki67
B
Vehicle
GSK-PKI
Ki67
C
Ki67+ cells [%]
***
Vehicle
KIRA8
D
Ki67+ cells [%]
*
Vehicle
GSK-PKI
E
Vehicle
KIRA8
Cl-Caspase 3
F
Vehicle
GSK-PKI
Cl-Caspase 3
G
Cl Caspase-3+/10^4 cells
*
Vehicle
KIRA8
H
Cl Caspase-3+/10^4 cells
**
Vehicle
GSK-PKI
I
Relative mRNA Expression
**
****
*****
****
Vehicle
KIRA8
Bip
Ire1α
Txnip
Bim
J
Spliced Xbp1 [%]
*
Vehicle
GSK-PKI
K
Relative mRNA Expression
*
*
Vehicle
GSK-PKI
Ins1
Ins2

Figure 7

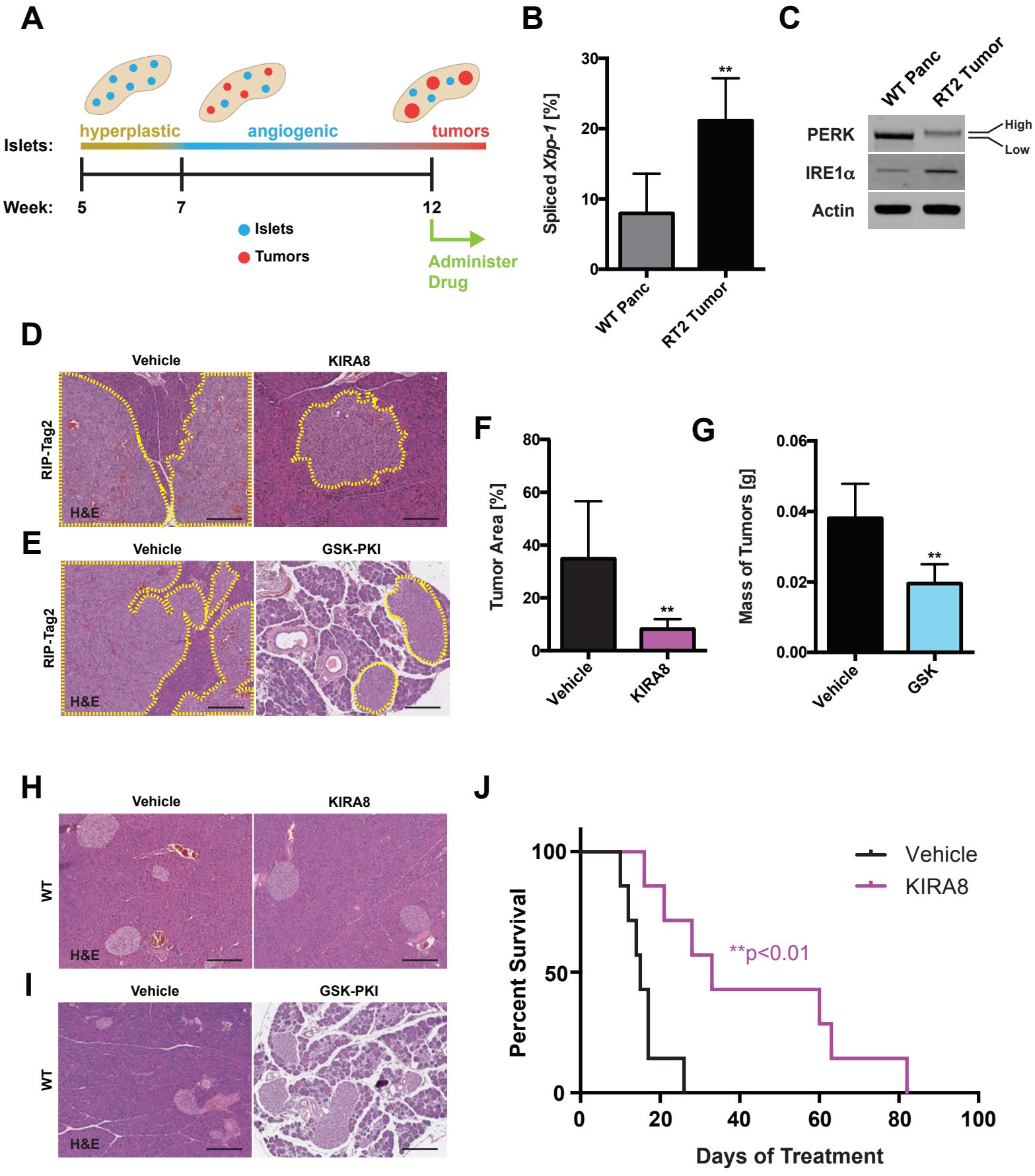
A
hyperplastic
angiogenic
tumors
Islets:
Week:
5
7
12
Islets
Tumors
Administer Drug
B
Spliced Xbp-1 [%]
30
20
10
0
**
WT Panc
RT2 Tumor
C
WT Panc
RT2 Tumor
PERK
IRE1α
Actin
High
Low
D
Vehicle
KIRA8
RIP-Tag2
H&E
E
Vehicle
GSK-PKI
RIP-Tag2
H&E
F
Tumor Area [%]
80
60
40
20
0
**
Vehicle
KIRA8
G
Mass of Tumors [g]
0.06
0.04
0.02
0.00
**
Vehicle
GSK
H
Vehicle
KIRA8
WT
H&E
I
Vehicle
GSK-PKI
WT
H&E
J
Percent Survival
100
50
0
0
20
40
60
80
100
Days of Treatment
Vehicle
KIRA8
**p<0.01

Figure 8

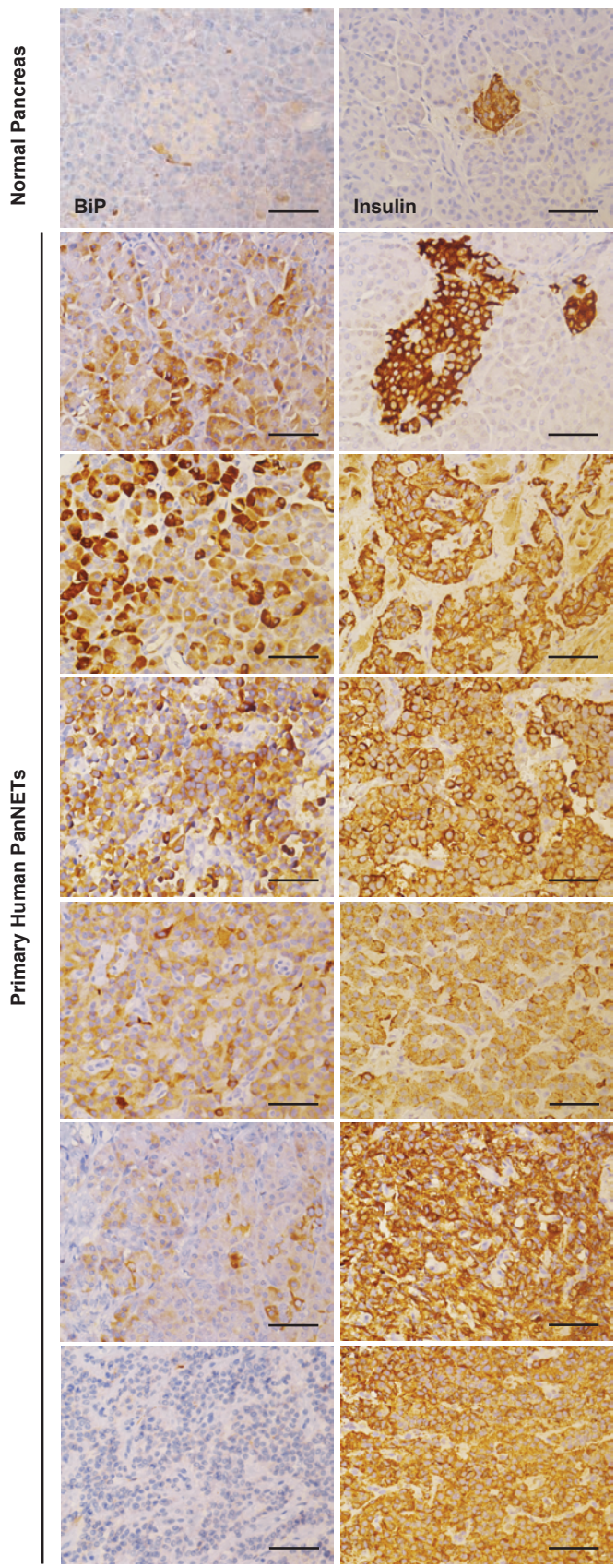

Figure S1

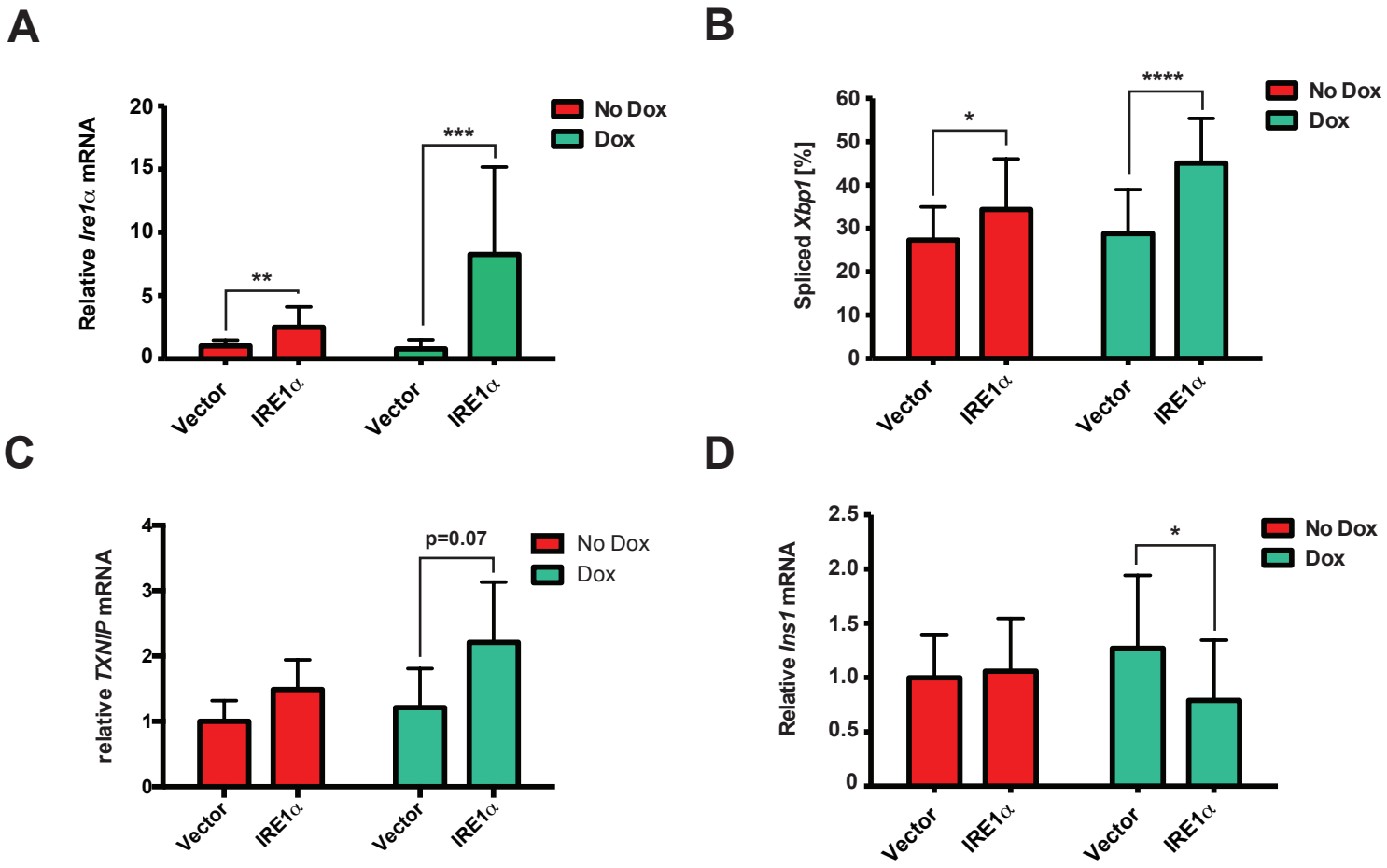
A
Relative Ire1α mRNA
20
15
10
5
0
**
***
No Dox
Dox
Vector
IRE1α
Vector
IRE1α
B
Spliced Xbp1 [%]
60
50
40
30
20
10
0
*
****
No Dox
Dox
Vector
IRE1α
Vector
IRE1α
C
relative TXNIP mRNA
4
3
2
1
0
p=0.07
No Dox
Dox
Vector
IRE1α
Vector
IRE1α
D
Relative Ins1 mRNA
2.5
2.0
1.5
1.0
0.5
0
*
No Dox
Dox
Vector
IRE1α
Vector
IRE1α

Figure S2

A

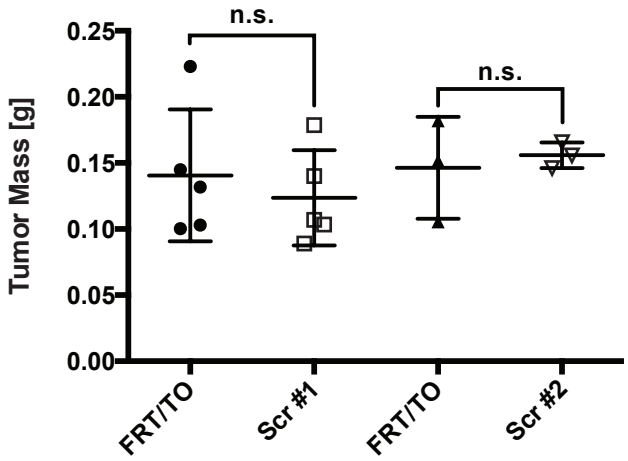
n.s.
n.s.
Tumor Mass [g]
0.25
0.20
0.15
0.10
0.05
0.00
FRT/TO
Scr #1
FRT/TO
Scr #2

Figure S3

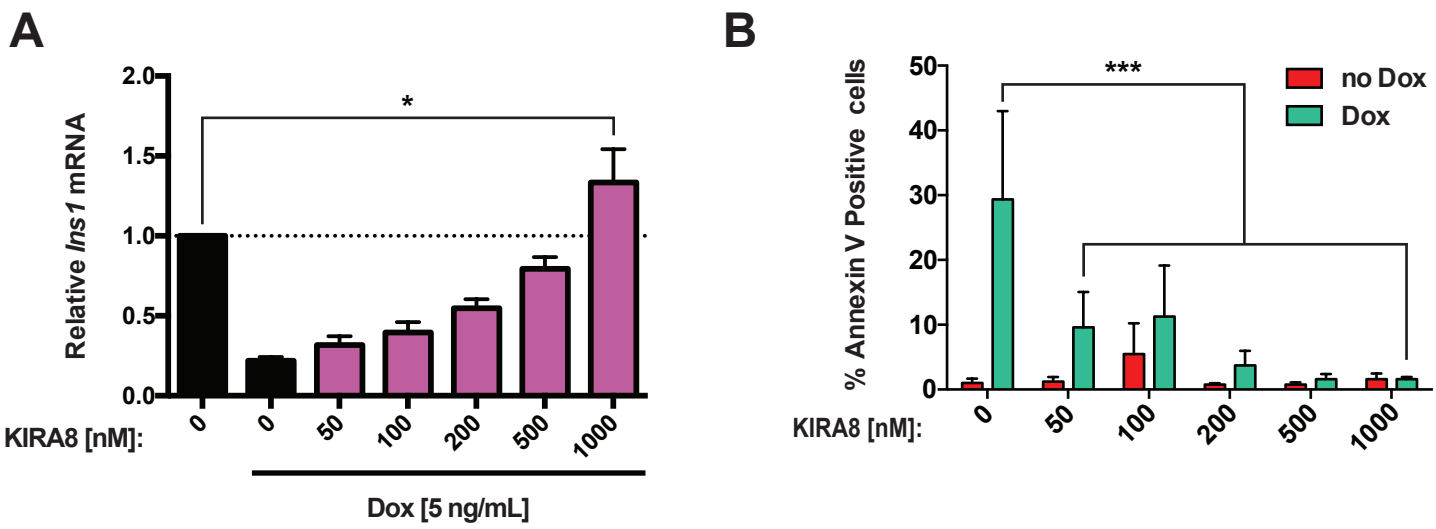
A
Relative Ins1 mRNA
2.0
1.5
1.0
0.5
0.0
*
KIRA8 [nM]:
0
0
50
100
200
500
1000
Dox [5 ng/mL]
B
% Annexin V Positive cells
50
40
30
20
10
0
***
no Dox
Dox
KIRA8 [nM]:
0
50
100
200
500
1000

Figure S4

A

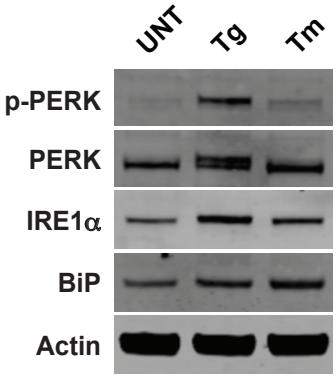

Figure S5

A

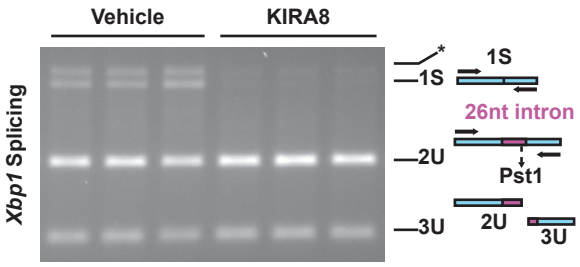
Vehicle
KIRA8
Xbp1 Splicing
1S
1S
26nt intron
2U
Pst1
3U
2U
3U

Figure S6

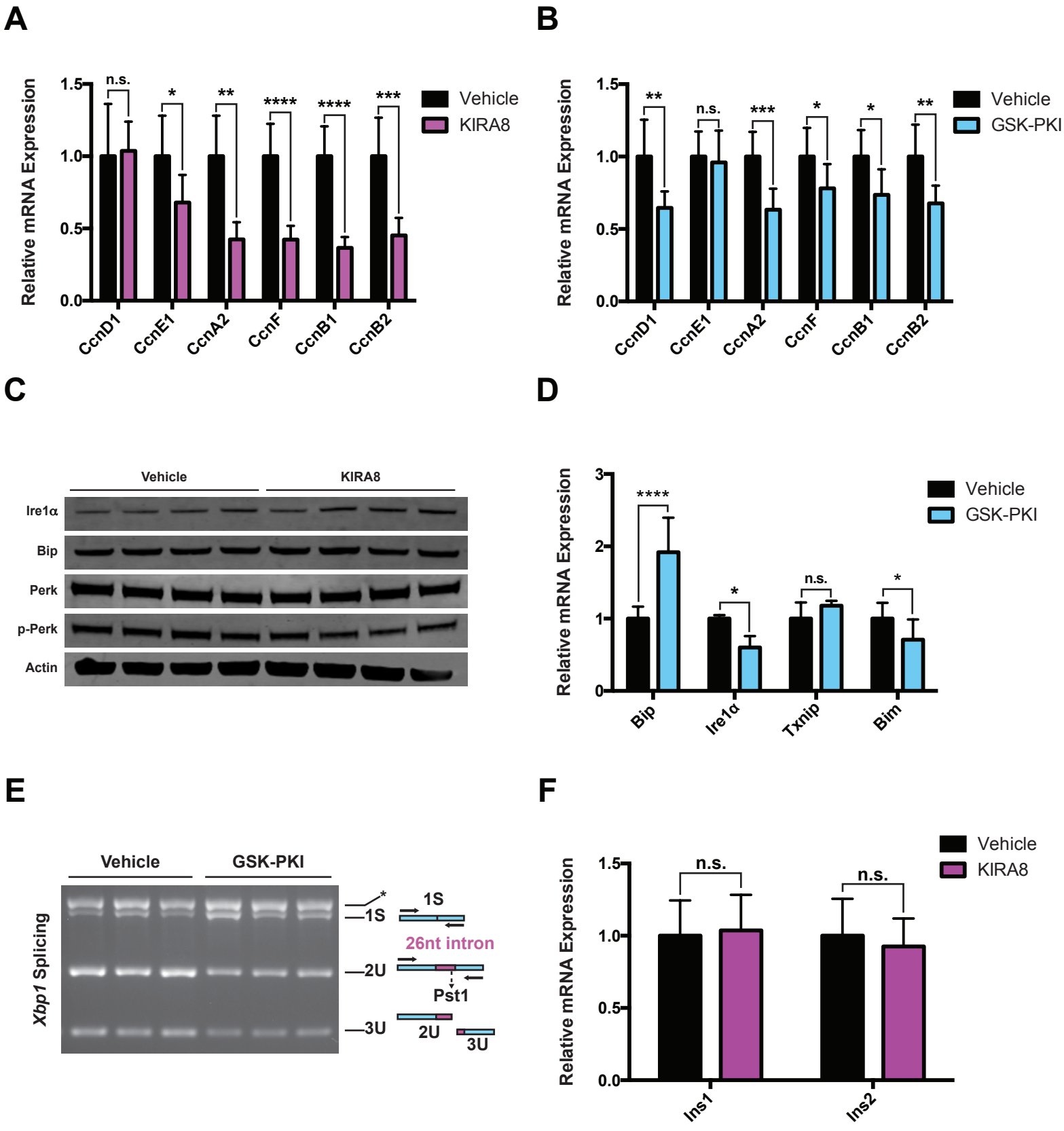
A
Relative mRNA Expression
1.5
1.0
0.5
0.0
n.s.
*
**
****
****
***
Vehicle
KIRA8
CcnD1
CcnE1
CcnA2
CcnF
CcnB1
CcnB2
B
Relative mRNA Expression
1.5
1.0
0.5
0.0
**
n.s.
***
*
*
**
Vehicle
GSK-PKI
CcnD1
CcnE1
CcnA2
CcnF
CcnB1
CcnB2
C
Vehicle
KIRA8
Ire1α
Bip
Perk
p-Perk
Actin
D
Relative mRNA Expression
3
2
1
0
****
*
n.s.
*
Vehicle
GSK-PKI
Bip
Ire1α
Txnip
Bim
E
Vehicle
GSK-PKI
Xbp1 Splicing
*
1S
1S
26nt intron
2U
Pst1
3U
2U
3U
F
Relative mRNA Expression
1.5
1.0
0.5
0.0
n.s.
n.s.
Vehicle
KIRA8
Ins1
Ins2

Figure S7

Supplementary Legends

Figure S1. Majority of Primary Human PanNETs Show Elevated ER Stress, Related to Figure 1

(A) IHC for BiP/GRP78 (left) and insulin (right) on normal human pancreas (top row) and a panel of six primary human PanNETs (Scale bars, 50 μm).

Figure S2. Manipulation of IRE1α adaptive vs. apoptotic signaling determines growth of INS-1 xenograft tumors, Related to Figure 2

A) NSG mice were subcutaneously injected with INS-1 (vector) cells or INS-1 cells carrying a doxycycline (Dox)-inducible, Myc-tagged Ire1α gene (INS-1::Ire1α). Mice were fed regular or Dox chow as shown in Figure 1F, and *Ire1α* mRNA levels were quantified after 4 weeks (n ≥ 13; mean ± SD; unpaired *t* tests).

(B) Percent spliced *Xbp1* in INS-1 xenograft tumors at 4 weeks post-injection (n ≥ 13; mean ± SD; unpaired t tests).

(C) mRNA levels of *Txnip* in INS-1 xenograft tumors treated +/- Dox for 96 hours at 2 weeks post-injection (n ≥ 5; mean ± SD; unpaired *t* tests).

(D) mRNA levels of *Ins1* in INS-1 xenograft tumors at 4 weeks post-injection.

*p<0.05, **p<0.01, ***p<0.001, ****p<0.0001 for (A-D)

Figure S3. Scrambled CRISPR Controls Do Not Decrease INS-1 Tumor Burden, Related to Figure 3

(A) NSG mice were injected with INS-1 control and one of two unique scrambled (Scr) CRISPR control clones. Resulting tumors were harvested and weighed at 4 weeks post-injection (n ≥ 3; individual values and mean ± SD; unpaired *t* tests).

n.s. = not significant

Figure S4. KIRA8 Reverses RIDD *In Vitro*, Related to Figure 4

(A) mRNA levels of *Ins1* in INS-1 IRE1α cells treated with the indicated concentrations of KIRA8 and doxycycline (Dox) for three days (n = 4; mean ± SD; paired *t* test)

(B) Percentage of INS-1 IRE1α cells stained with Annexin V-FITC after three days of treatment with 10 ng/mL Dox and the indicated concentrations of KIRA8 (n = 8; mean ± SD; paired *t* tests).

*p<0.05, ***p<0.001 for (A) and (B)

Figure S5. Thapsigargin Activates Both IRE1α and PERK *In Vitro*, Related to Figure 5

(A) Immunoblots with the indicated antibodies of lysates prepared from INS-1 cells treated for 16 hours with DMSO (UNT), 31.25 nM thapgsigargin (Tg), or 500 ng/mL tunicamycin (Tm).

Figure S6. KIRA8 Inhibits *Xbp1* Splicing *In Vivo*, Related to Figure 6

(A) Representative DNA gel of the spliced (1S) and unspliced (2U and 3U) *Xbp1* amplicons after PstI treatment. Quantified in Figure 5A.

Figure S7. KIRA8 and GSK-PKI Induce Distinct Apoptotic Markers in INS-1 Tumors, Related to Figure 7

(A) Levels of the indicated mRNAs from tumors in Figure 6A (n = 8; mean ± SD; unpaired *t* tests).

(B) Levels of the indicated mRNAs from tumors in Figure 6B (n = 8; mean ± SD; unpaired *t* tests).

(C) Immunoblots with the indicated antibodies of tumors in Figure 6A.

(D) Levels of the indicated mRNAs from tumors in Figure 6B (n ≥ 3; mean ± SD; unpaired *t* tests).

(E) Representative DNA gel of the spliced (1S) and unspliced (2U and 3U) *Xbp1* amplicons after PstI treatment. Quantified in Figure 6J.

(F) *Ins1* and *Ins2* mRNA levels in tumors from Figure 6A (n = 8; mean ± SD; unpaired *t* test).

*p<0.05, **p<0.01, ***p<0.001, ****p<0.0001, n.s. = not significant for (A), (B), (D) and (F)

Figure S8. Effects of KIRA8 and GSK-PKI on WT C57BL/6 mice, Related to Figure 8

(A and B) Masses of pancreata from 14-week-old wild-type C57BL/6 mice after 14 days of treatment with (A) 50 mg/kg/d KIRA8, (B) 50 mg/kg/d GSK-PKI, or the corresponding vehicle (n ≥ 5; mean ± SD; unpaired *t* test).

*p<0.05, n.s. = not significant for (A) – (D)

Experimental Procedures

Human Samples

We obtained 6 formalin-fixed paraffin-embedded (FFPE) samples of de-identified primary human PanNETs, 4 frozen human PanNET samples for RNA analysis, and matched normal pancreata from the UCSF Department of Pathology, IRB protocol number 13-11606

Tissue Culture

INS-1 cell lines were cultured in RPMI-1640 media supplemented with 10% tetracycline-free FBS (Gemini Bioproducts), 10 mM HEPES, 2 mM Glutamine, 110 µg/mL Na Pyr, 100 U/mL penicillin, 100 ug/mL streptomycin (UCSF Cell Culture Facility) and 100 µM BME (Bio Rad). Generation of isogenic, stable INS-1 lines was performed as previously described [9]. Brefeldin A (BFA), tunicamycin, thapsigargin and doxycycline were purchased from Sigma-Aldrich.

Small Molecules

KIRA8 and was synthesized in house and purified by reverse phase chromatography (HPLC). The purity of KIRA8 was determined with two analytical RP-HPLC methods, using a Varian Microsorb-MV 100-5 C18 column (4.6 mm x 150 mm), and eluted with either H2O/CH3CN or H2O/ MeOH gradient solvent systems (+0.05% TFA) run over 30 min. Products were detected by UV at 254 nm. KIRA8 was found to be >95% pure in both solvent systems. GSK2656157 (GSK-

PKI) was purchased at >98% purity from Advanced Chemblocks Inc. (Burlingame, CA). For use in tissue culture, KIRA8 and GSK-PKI stock solutions were prepared by dissolving in DMSO at a concentration of 20 mM. For use in animal studies, KIRA8 was dissolved in a vehicle solution of 3% ethanol, 7% Tween-80, 1.2% ddH_2O, and 88.8% of 0.85% W/V saline at a working concentration of 10 mg/ml; GSK-PKI was dissolved in 5% 1-methyl-2-pyrrolidinone (NMP), 5% Kolliphor HS 15 (Solutol), and 90% of 20% W/V (2-Hydroxypropyl)-β-cyclodextrin (HP-β-CD) at a working concentration of 10 mg/mL.

CRISPR/Cas9

Guide RNAs were designed using the Zhang Lab's Optimized Design Tool (crispr.mit.edu) and targeted to the 5' end of each gene to create random insertions/deletions (indels) upstream of key structural and functional domains. For each gRNA, forward and reverse oligonucleotides were purchased from Integrated DNA Technologies (Table S1), annealed, and ligated into the pSpCas9(BB)-2A-EGFP vector (pX458; a gift from Feng Zhang; Addgene Plasmid #48138) at the BbsI cloning site. The resulting plasmids were transfected into INS-1 cells using Lipofectamine 2000 (Thermo Fisher Scientific); a BD FACSAria II (BD Biosciences) was used to subsequently single-cell sort EGFP-positive cells and establish clonal lines. Clones were screened for knockout of target genes by Western Blot and/or by allelic sequencing with custom primers (Integrated DNA Technologies; Table S2) after processing genomic DNA with the KAPA Mouse Genotyping Kit (KAPA Biosystems) and TOPO TA Cloning Kit (Life Technologies).

Western Blot and Antibodies

For protein analysis, cells were lysed in T-PER buffer (Thermo Fisher Scientific) plus phosphatase inhibitor cocktail (Cell Signaling Technologies). Protein concentration was determined using Pierce BCA Protein Assay (Thermo Fisher Scientific). Western blots were performed using 10% and 4-12% gradient Bis-Tris precast gels (NuPage) on Invitrogen XCell SureLock Mini-Cell modules. Gels were run using 2-(N-morpholino)ethanesulfonic acid (MES) buffer (Invitrogen) and transferred onto nitrocellulose transfer membrane using an XCell II Blot Module or iBlot Dry Blotting System (Thermo Fisher Scientific). Antibody binding was visualized on CL-XPosure film using ECL SuperSignal West Extended Duration Substrate (both from Thermo Fisher Scientific) or using the Odyssey CLx Imaging System (LI-COR Biosciences). Antibodies used: IRE1α (Cell Signaling Technology #3294), PERK (CST #3192), PERK p-T980 (CST #3179), BiP (CST # 3177), Spliced XBP-1 (BioLegend #619502), actin (Sigma A5441 1:3000), CHOP (CST #2895).

RNA Isolation, Quantitative Real-Time PCR, and Primers

RNA was isolated from whole cells using either Qiashredder and RNeasy kits (Qiagen) or Trizol (Invitrogen). TissueLyser LT (Qiagen) was used for RNA isolation from tumors. For cDNA synthesis, 500-1000 ng total RNA was reverse transcribed using Superscript II Reverse Transcriptase and Oligo $d(T)_{16}$ primer (Invitrogen). For qPCR, we used Power SYBR Green and the StepOnePlus Real-

Time PCR System (Applied Biosystems). qPCR primers are listed in Table S3. Gene expression levels were normalized to Actin; GAPDH control also used where indicated.

XBP-1 mRNA splicing

RNA was isolated from whole cells or tissue and reverse transcribed as detailed above to obtain total cDNA. Sense (5'-AGGAAACTGAAAAACAGAGTAGCAGC-3') and antisense (5'-TCCTTCTGGGTAGACCTCTGG-3') primers were used in a standard GoTaq Green PCR reaction (Promega) to amplify a region spanning the 26-nucleotide intron that includes a single PstI restriction site, which is excised by active IRE1α. The resulting PCR fragments were then digested by PstI (New England Biolabs), resolved on 3% agarose gels, stained with ethidium bromide and quantified by densitometry using ImageJ (U. S. National Institutes of Health).

Cell Growth and Apoptosis Assays

To measure apoptosis by Annexin V staining, cells were plated in 12-well plates overnight. Cells were then treated as described for indicated times. On the day of analysis, cells were trypsinized, washed in PBS, and resuspended in Annexin V binding buffer (10 mM HEPES 7.4, 140 mM NaCl, 2.5 mM $CaCl_2$) with Annexin-V FITC (BD Biosciences). Flow cytometry was performed on a Becton Dickinson LSRFortessa or LSRII flow cytometer. To measure cell proliferation, cells were seeded at 5-10% confluence in 96-well plates, treated as indicated, and assayed using the CellTiter-Glo Luminescent Cell Viability Assay (Promega) according to

the manufacturer's protocol. Luminescence was quantified using a Cytation 5 Cell Imaging Multi-Mode Reader (BioTek).

Animal Studies

All animal studies were reviewed and approved by the UCSF Institutional Animal Care and Use Committee. Animals were maintained in a specific pathogen-free animal facility on a 12hr light–dark cycle at an ambient temperature of 21°C. They were given free access to water and food.

Xenografts

5-8 week old NOD.Cg-*Prkdc*^{scid} *Il2rg*^{tm1Wjl}/SzJ (NSG, Stock #005557, The Jackson Laboratory) mice were injected subcutaneously with 5 x 10^6 INS-1 cells, and tumor size was followed for up to 4 weeks. Where indicated, animals were provided doxycycline chow (Envigo TD.09761). For small molecule studies, KIRA8, GSK-PKI or the corresponding vehicle solutions were prepared as described above and delivered daily by intraperitoneal injection.

RIP-Tag2

Tg(RIP1-Tag)2Dh mice (previously described in (Hanahan, 1985)) were initially obtained from the Bergers Lab at UCSF and maintained as heterozygotes by breeding wild-type C57BL/6 female mice with hemizygous RIP-Tag2 male mice. RIP-Tag2-positive mice were given supplemental diet with adjusted sucrose starting at 12 weeks (Envigo TD.86489). KIRA8 and GSK-PKI treatments, as

described above, were initiated at 12 weeks and continued as described.

Blood Collection and Protocols

To monitor blood glucose levels, a drop of blood was collected from the tail onto OneTouch® Ultra® Blue test strips and measured using the OneTouch® Ultra® 2 Meter (LifeScan). For complete blood counts, blood was collected by retro-orbital bleed into EDTA-coated tubes (BD #365974) and analyzed on a Hemavet 950.

Histology and Immunostaining

Samples were fixed in 4% buffered formaldehyde for 24h, washed in PBS, transferred into 70% EtOH in ddH_2O, and then embedded in paraffin and sectioned (5mm thickness) using a Leica RM2255 rotary microtome or by the Brain Tumor Research Center (BTRC) Histology Core at UCSF. Hematoxylin and eosin staining was performed using standard methods. Stained slides were imaged using an Aperio AT2 slide scanner and data were processed using QuPath software. Total cell counts and Ki67 stains were automated; all other images were quantified manually in a blinded fashion. Antibodies used for immunohistochemistry: BiP [C50B12] (Cell Signaling Technology #3177, 1:200), CD31 (CST #77699 1:100), Chromogranin A [polyclonal] (Cell Marque, 1:4), Cleaved Caspase-3 (CST #9661 1:200), Insulin (DAKO A0564, 1:200), IRE1α (CST #3294, 1:100), Ki67 (Ventana #790-4286, Undiluted), Myc (Sigma M4439, 1:5000), Synaptophysin [LK2H10 clone] (Cell Marque, 1:100).

Statistics

Statistical analyses are expressed as means +/- standard deviation. Significance was determined by two-tailed Student's *t*-test or logrank (Mantel-Cox) test; *P* values < 0.05 were considered statistically significant. Graphs were generated using Prism 6 software and represent the average of at least 3 independent experiments.

Table S1. CRISPR/Cas9 guide Oligos

Gene	Forward Sequence 5'-3'	Reverse Sequence 5'-3'
Ire1α #1	caccGCAAGAGGACAGGCTCCATCAAG	aaacCTTGATGGAGCCTGTCCTCTTGC
Ire1α #2	caccTGCCTGAACCAATTCCGGGA	aaacTCCCGGAATTGGTTCAGGCA
Perk #1	caccAGATGGACGAATTGCCGCAC	aaacGTGCGGCAATTCGTCCATCT
Perk #2	caccCGCGCGTGACTCCTGTTCGC	aaacGCGAACAGGAGTCACGCGCG
Scr #1	caccGCACTACCAGAGCTAACTCA	aaacTGAGTTAGCTCTGGTAGTGC
Scr #2	caccCCCCTTCGACCAGTCGGGTT	aaacAACCCGACTGGTCGAAGGGG
Xbp1 #1	caccTTCCGGGCCCGCGAGCCGCA	aaacTGCGGCTCGCGGGCCCGGAA
Xbp1 #2	caccGTTCCGGGCCCGCGAGCCGC	aaacGCGGCTCGCGGGCCCGGAAC

Table S2. Genotyping/Sequencing Primers

Gene	Forward Sequence 5'-3'	Reverse Sequence 5'-3'
Ire1α	TACAGGGCCATTTGAGGGAG	CGATCTCTCCAGCCCGAGTA
Xbp1	GCCTGCAGGACCAATAAACG	GCGAATCTAACCCACCGTGA
Perk	GGAACCCTCGCTCAATGGG	CGAAACAATGAAAGCGGGGAA

Table S3. qPCR Primers

Species	Gene	Forward Sequence 5'-3'	Reverse Sequence 5'-3'
Human	ATF4	GTTCTCCAGCGACAAGGCTA	ATCCTCCTTGCTGTTGTTGG
Rat	Actin	GCAAATGCTTCTAGGCGGAC	AAGAAAGGGTGTAAAACGCAGC
	Bim	CGGATCGGAGACGAGTTCAA	TAACCATTTGCGGGTGGTCT
	Bip	ATCGACTTGGGGACCACCTA	AGTGAAGGCCACATACGACG
	Gapdh	CAGGGCTGCCTTCTCTTGTG	AACTTGCCGTGGGTAGAGTC
	Ins1	GTCCTCTGGGAGCCCAAG	ACAGAGCCTCCACCAGG
	Ins2	GGGAGCGTGGATTCTTCTACAC	CCACTTGTGGGTCCTCCACTT
	Ire1α	GTCCCACTTTGTGTCCAATGG	TCCCCAGACATGAAGGTCA
	Txnip	CTGATGGAGGCACAGTGAGA	CTCGGGTGGAGTGCTTAGAG